5-2011

JOULE HEATING EFFECTS ON ELECTROKINETIC TRANSPORT IN CONSTRICTION MICROCHANNELS

Sriram Sridharan
Clemson University, srirams@g.clemson.edu

JOULE HEATING EFFECTS ON ELECTROKINETIC TRANSPORT IN CONSTRICTION MICROCHANNELS

A Thesis
Presented to
The Graduate School of
Clemson University

In Partial Fulfillment
of the Requirements for the Degree
Master of Science
Mechanical Engineering

---

by
Sriram Sridharan
May 2011

Accepted by:
Dr. Xiangchun Xuan, Committee Chair
Dr. Richard Miller
Dr. Gang Li

ABSTRACT

Microfluidic technology involving multidisciplinary studies including MEMS, chemistry, physics, fluids and heat transfer has been developed into a promising research field in the recent decade. If offers many advantages over conventional laboratory techniques like reduced reagent consumption, faster analysis, easy fabrication and low chemical waste. Microfluidic lab-on-a-chip devices have been used to manipulate cells and particles like sorting, separating, trapping, mixing and lysing. Microfluidic manipulation can be achieved through many methods and insulator based dielectrophoresis (iDEP) is one of the highly used method in the recent years. In iDEP, both DC and AC voltages can be applied to the remote electrodes positioned in end-channel reservoirs for transporting and manipulating particles. The electric field gradients are caused by the blockage of electric current due to in-channel hurdles, posts, and ridges. However, iDEP devices suffer from the issue of Joule heating due to locally amplified electric field around the insulators.

A parametric study of Joule heating effects on electroosmotic fluid flow in iDEP is studied under various electric fields. It was determined that depending upon the magnitude of DC voltage, a pair of counter rotating vortices fluid circulations can occur at either downstream end or each end of the channel constriction. Moreover, pair at the downstream end appears larger in size than the upstream end due to DC electroosmotic flow. A numerical model is

developed to simulate the fluid circulations occurred due to the action of electric field on Joule heating induced fluid inhomogeneities in the constriction region.

Focusing particles or cells into a single stream is usually a necessary step prior to counting and separating them in microfluidic devices such as flow cytometers and cell sorters. A systematic study of Joule heating effects on electrokinetic particle transport in constriction microchannels under DC and DC biased AC electric fields is presented in this work. A numerical model is developed to capture the particle trace observed in the experiments. It was determined that particle transport is greatly affected by electrothermal effects where Joule heating is high. At very low DC magnitude where the electrothermal effects dominate the electrokinetic flow, particles in the shallow depth channel are being trapped and particles in deep channels are transported to the downstream reservoir from the constriction in a single streamline.

Electrothermal flow circulations should be taken into account in the design and operation of iDEP devices, especially when highly conductive solutions and large electric fields must be employed. They may potentially be harnessed to enhance microfluidic mixing and immunoassay for lab-on-a-chip applications. A numerical study of Joule heating effects on the sample mixing performance in constriction microchannels is presented in this work. It was determined that Joule heating induced electrothermal force enhanced the sample mixing by generating circulations at the ends of the constriction under DC biased AC electric fields. Furthermore, mixing performance was also studied for various parameters like

applied electric field, channel structure, channel depth and number of constrictions.

ACKNOWLEDGEMENTS

I would like express my sincere gratitude to my advisor Dr. Xiangchun Xuan for his continuous support and valuable guidance throughout my graduate studies. His thoughtful guidance has helped me in the research and writing this thesis. I am thankful for the grading assistantships he provided to fund my living expenses. I am also thankful to my committee members Dr. Richard Miller and Dr. Gang Li for their valuable inputs.

Besides my advisor, I would like to thank Junjie Zhu for his valuable information he gave me about the experiments and helping me in learning the COMSOL multiphysics software tool. I also thank my fellow mates in the research group: Litao Liang, Bhaskar Ramesh, Saurin Patel, Amit Srivatsva and Srijeeth Sathyamoorthy who have been supportive in my work.

Finally, I would like to thank my family for their continual love and support during my graduate career.

TABLE OF CONTENTS

LIST OF TABLES

Tables Page

LIST OF FIGURES

NOMENCLATURE

r	Ratio of the DC to AC voltage
c	Numerical modeling correction factor
ζ_w	Wall zeta potential
ζ_p	Particle zeta potential
ε_0	Permittivity of vacuum
ε_r	Relative permittivity of the fluid
σ_p	Electric conductivity of the particle
σ_m	Electric conductivity of the fluid
ϕ	Electric potential
E	Electric field
F_{CM}	Clausius–Mossotti (CM) factor
F_{DEP}	Dielectrophoretic force
a	Radius of the particle
η	Viscosity of the fluid
μ_{DEP}	dielectrophoretic mobility
μ_{EK}	electrokinetic mobility
u_{eo}	Electroosmotic velocity
u_{ep}	Electrophoretic velocity
U_{EK}	Electrokinetic velocity

U_{DEP} Dielectrophoretic velocity

U_p Particle velocity

Q Joule heating

ρ_e Free charge density

f Electrical body force

ω Angular frequency

k Thermal conductivity

C_p Specific heat

ρ Fluid density

α Linear temperature coefficient of fluid permittivity

β Linear temperature coefficient of fluid conductivity

T_0 Reference temperature

h Heat transfer coefficient

q'' Outward heat flux

D Diffusion coefficient

c Sample concentration

ξ Efficiency of mixing

CHAPTER 1

INTRODUCTION

1.1 Objective and motivation

With the advent of easy micro-fabrication techniques, there has been an increasing development in the lab-on-a-chip (LOC) micro fluidic technology in the same way as a microelectronic chip in a computer. A lab-on-a-chip is a device that integrates several laboratory functions into a single chip of centimeters in size and built on a thin glass plate with network of microchannels, electrodes, sensors and circuits. Elastomer materials like poly(dimethylsiloxane) (PDMS) have emerged as a better replacement to the older glass and silicon based devices. LOC devices can perform the room-sized functions of clinical diagnosis of bacteria, viruses and DNA in a micro level. The most basic LOC fabrication process is the photolithography method. With the growing demands of faster prototyping and lower production cost several methods like soft lithography and stereo lithography have been developed. The main advantage of LOCs is the low fluid volume consumption, faster analysis and response time, low fabrication costs, safer platform for biological, chemical studies and better process control. This chapter begins with a brief introduction about microfluidics and some of the basic electrokinetic phenomenon which are responsible for the fluid transport in microfluidics [1].

Microfluidics deals with the precise control and manipulation of fluids and particles which are constrained to a micro scale. The width and height of

microfluidic chip vary from 20 to 200 µm. It provides a perfect platform for multidisciplinary studies like physics, chemistry, MEMS, mechanics and biotechnology. Microfluidic approach started from the early days of manufacturing of inkjet printers. With the recent advancement in microfluidics it has found wide applications in the areas of pharmaceuticals, life science and biotechnology. Microfluidics offer many benefits like reduction in size and reagent volumes from liters to nano liters. Reactions happen much faster in a small scale and thus leading to easy manipulation of cells and particles like focusing, trapping and mixing. In focusing, dispersed particles at the microchannel entrance are constrained into a single stream at the exit of the microchannel. Trapping refers to the restriction of the particle movement at high electric field regions in the microchannel. Finally, mixing refers to the diffusion of two fluid streams at a junction when introduced from different inlets [2, 3].

Microfluidic manipulation can be achieved through many methods and insulator based dielectrophoresis (iDEP) is one of the highly used method in the recent years. In iDEP, both DC and AC voltages can be applied to the remote electrodes positioned in end-channel reservoirs for transporting and manipulating particles. The electric field gradients are caused by the blockage of electric current due to in-channel hurdles, posts, and ridges. Although electrokinetic process enhance species transport and better flow control there exist an inevitable Joule heating generated within the fluid when an axial electric field is applied in the microchannel. Joule heating magnifies in the regions of locally

amplified electric field as it is proportional to the electric field square. This internally generated heat can lead to a significant increase in the liquid temperature and affect the electrokinetic transport. The thesis is categorized into 3 chapters and each chapter discussing the specific electrokinetic transport process based on the induced Joule heating. Chapters 2 deals with the Joule heating effects on the electroosmotic flow in an insulator based dielectrophoresis. Chapter 3 deals with the Joule heating effects on electrokinetic particle transport in two different sizes of microchannels. Finally, chapter 4 explains the Joule heating effects on the electrokinetic transport of sample mixing.

1.2 Electrokinetic phenomena

Application of electric fields along the microchannel controls the movement of bulk fluid and the particles through phenomenon like electrophoresis, electro-osmosis and dielectrophoresis etc. These phenomena are used in the microfluidics to manipulate particles and cells like focusing, trapping and separating them. According to the type of electric field, electro-kinetics is divided into DC electro-kinetics and AC electro-kinetics. In DC electro-kinetics, there are DC electro-osmosis, DC electrophoresis and Joule heating effect caused by high DC voltage. Likewise, AC electro-kinetics includes AC electro-osmosis, dielectrophoresis and electrothermal flow. This is explained in the following fig.1-1. The subheading following this paragraph explains few of the concepts that are of important to the objective of the work presented in the following chapters [1].

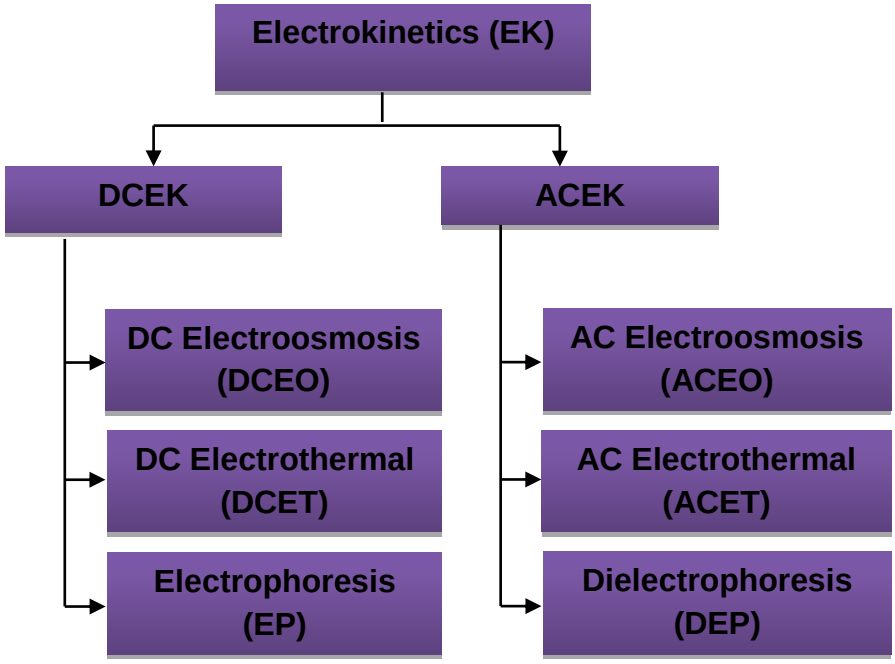

Fig. 1-1: Electrokinetic mechanisms [5]

1.2.1 Electric Double Layer

Electrical double layer (EDL) is the fundamental phenomenon for the electrokinetic transport in a microchannel. When electrolytes are present in water electro-neutrality condition is achieved at locations far away from the container's walls under no flow conditions. However when a glass slide or any slid substance is immersed in an electrolyte solution with a surface charge on it, the charged surface will affect the distribution of nearby ions in the electrolyte solution. Ions of opposite charge will be attracted to the surface and the like charges are repelled away from the surface. As a consequence of attraction and repulsion of ions near the surface a non-uniform distribution of ions formed normal to the surface which means there will be high concentration of counter-ions near the surface and co

ions will be distributed far away from the surface exhibiting electro-neutrality condition. Such redistribution gives rise to the formation of electrical double layer. From the double layer to the electro-neutral solution the net charge density gradually reduces to zero [1]. A typical formation of EDL is being presented in the fig1-2.

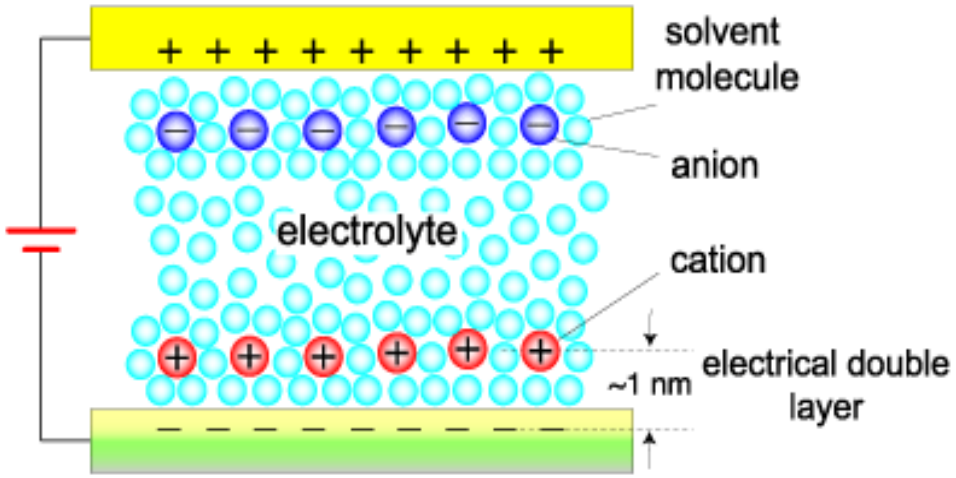

Fig. 1-2: Illustrates the formation of electrical double layer [4].

1.2.2 Electroosmosis

Electroosmotic flow is the movement of bulk electrolyte solution relative to a stationary charged surface under the influence of electric field. When a surface is negatively charged and an electric field applied tangentially to the surface, the negatively charged surface attracts positive ions and repels negative ions from the surface. As a result of orientation of positive and negative ions there will be a non-uniform ionic distribution normal to the surface leading to the formation of electrical double layer. The applied electric field exerts a force on the excess ions

in the diffuse part of the double layer and drags the electrolyte solution along with them. The flow is termed to be electro-osmotic flow [6].

Electro-osmotic velocity is represented as

$$u_{eo} = -\frac{\varepsilon\zeta}{\eta}\boldsymbol{E} \tag{1}$$

$$\mu_{eo} = -\frac{\varepsilon\zeta}{\eta} \tag{2}$$

Where, u_{eo} is the electro-osmotic velocity in m/s, μ_{eo} is the electro-osmotic mobility in $m^2/V\ s$, ε is the permittivity of the fluid in F/m, ζ is the zeta potential in mV and η is the viscosity of the fluid in Pa s.

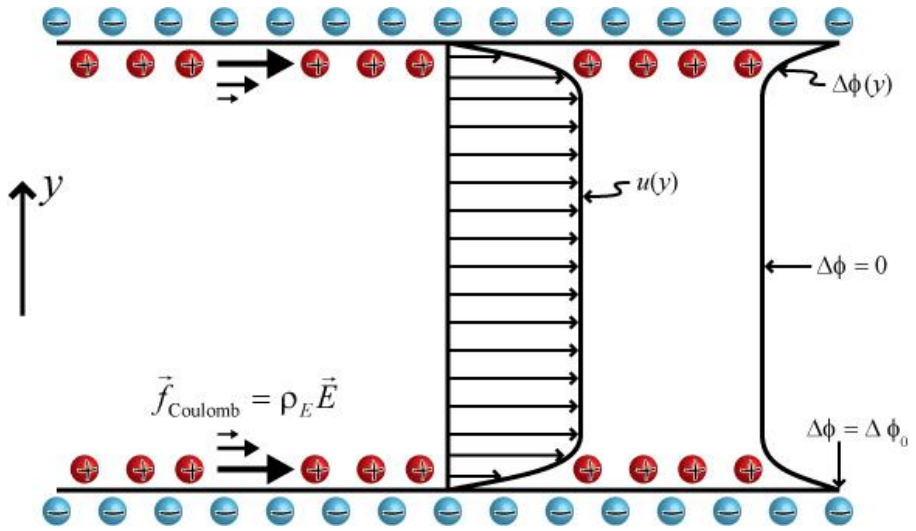

Fig. 1-3: Electroosmotic flow and the velocity profile in a slit microchannel when an electric field is applied [7].

1.2.3 Electrophoresis

Consider a particle in the bulk electrolyte solution. When electric field is applied electrostatic charge on the particle surface causes the particle to move

relative to the stationary or moving liquid. Such a motion is called electrophoresis. From the double layer principle, all surface charges in fluids are screened by a diffuse layer of ions, which has the same absolute charge but opposite sign with respect to that of the surface charge. The electric field also exerts a force on the ions in the diffuse layer which has direction opposite to that acting on the surface charge. The electrophoretic movement is always opposite in direction to electro-osmosis. It is used to separate molecules with different physical characteristics. As in typical case, the electro-osmotic motion dominates and the particles are dragged through the channel along with the bulk flow [6].

The electrophoretic velocity for a particle can be expressed as follows:

$$u_{ep} = -\frac{\varepsilon \zeta_{\mathrm{p}}}{\mu}(E) \tag{3}$$

where u_{ep} is the electrophoretic velocity, ε is again the dielectric constant of the liquid, ζ_{p} is the static surface charge of the particle, μ the fluid viscosity, and E is the applied electric field.

1.2.4 Dielectrophoresis

Dielectrophoresis refers to the response of an electrically polarized object (either charged or non-charged) in a non-uniform electric field. The strength of the force depends upon dielectric properties of the medium and the particles, particle shape and size, frequency of the electric field. As the electric field becomes non-uniform, particles experience variable dielectrophoretic forces, $\mathbf{F}_{DEP}$, when they move electro-kinetically through the microchannel. Using the

dipole moment approximation, dielectrophoretic force on the spherical particle is given by [3]

$$F_{DEP} = \pi\varepsilon(T)a^3 f_{CM}(E \bullet \nabla E) \quad (4)$$

$$f_{CM} = (\sigma_p - \sigma_f)/(\sigma_p + 2\sigma_f) \quad (5)$$

Where $\varepsilon(T)$ is the fluid permittivity, a is the radius of the particle, f_{CM} is the Clausius-Mossotti (CM) factor, **E** is electric field strength, σ_p the electric conductivity of particles, and σ_f the electric conductivity of the medium. It is important to note that Eq. (4) is valid only when the particle size is much smaller than the characteristic length scale of the electric field. Dielectrophoretic force is proportional to the diameter of the cell or particle. It is a highly used technique in separating particles and cells based on their size. This phenomenon is discussed in detail in chapter 3 of this thesis.

1.3 Concept of Joule heating

Joule heating is the electrical energy generated per unit volume. When a wire is immersed in a mass of water and electric current is applied temperature of the water increased due to the current flowing through the wire for a considerable length of time. Similarly, in micro channels, Joule heating is generated in electrolyte solutions of finite conductivity on application of AC and as well as DC fields. When voltage difference is applied at the electrodes, electric energy is consumed by resistive fluid as electric current flow through and transformed into heat. The heating is uneven in across the volume of bulk fluid. It causes

temperature gradients in the properties of the fluid and modifies the local conductivity and permittivity distributions which release heat in the channel. Heat generated due to joule heating is proportional to the square of electric field [8, 9]. Heat generation is expressed as

$$Q = \sigma(\mathbf{E} \bullet \mathbf{E}) \tag{6}$$

Where Q is the heat generated in W/m^3, σ is the electrical conductivity in S/m and **E** is the electric field in V/m.

1.4 Electrothermal body force

Electro-thermal flow is the motion of fluid due to the action of electric field on the Joule heating induced gradients of conductivity and permittivity in the fluid. Electro-thermal flow occurs in both AC and DC electro-kinetics and it is more prominently seen in AC electro-kinetics. In DC Electro-kinetics, electro-osmotic flow dominates and the electro-thermal flow cannot be observed even though it affects the electroosmotic plug like velocity profile and separation efficiency of particles and cells. When an AC voltage is applied at the electrodes, the non-uniform electric field causes joule heating in the channel. Joule heating creates temperature gradients in conductivity and permittivity of the electrolyte solution. As a result, an electrical body force is generated which causes the fluid to flow in a swirling pattern called electro-thermal flow [10, 40]. Such type of flow can be seen in a varied cross section channel. The time averaged electrical body force which is responsible for electrothermal flow is represented as

$$\boldsymbol{f} = \rho_e \boldsymbol{E} - 0.5\boldsymbol{E}^2 \nabla \varepsilon \quad (7)$$

Where, ρ_e is the volume charge density in C/m^3, **E** is the applied electric field in V/m and ε is the permittivity of the fluid.

CHAPTER 2

JOULE HEATING EFFECTS ON ELECTROOSMOTIC FLUID FLOW IN CONSTRICTION MICROCHANNELS

2.1 Introduction

As a versatile tool, dielectrophoresis (DEP) has been widely used to focus, trap, concentrate and separate cells, viruses, and biomolecules in microfluidic devices for various lab-on-a-chip applications [12-14]. DEP refers to the induced motion of particles (either charged or non-charged) in a non-uniform electric field [11]. The electric field gradients in these devices are created by either microelectrodes [15,16] or micro insulators [17-19]. In electrode-based dielectrophoresis (i.e., eDEP), pairs of microelectrodes are placed inside a microchannel. High-frequency AC voltages are supplied to achieve strong electric fields/gradients and suppress electrochemical reactions on electrode surfaces [20-27]. In insulator-based dielectrophoresis (i.e., iDEP), both DC and AC voltages (of any frequency) can be applied to the remote electrodes positioned in end-channel reservoirs for transporting and manipulating particles. The electric field gradients are caused by the blockage of electric current due to in-channel hurdles, posts, and ridges etc [28-37].

Both eDEP and iDEP suffer from the issue of Joule heating in the suspending medium due to the locally amplified electric field around micro electrodes or insulators (typically on the order of hundreds of kV/m) [38,39]. It

has been long known in capillary electrophoresis that Joule heating can elevate the buffer temperature and disturb the electroosmotic flow causing significant sample dispersion [40-43]. The effects of Joule heating on fluid temperature and motion in eDEP have been investigated previously [44-48]. It was reported that a pair of counter-rotating fluid circulations could form near the microelectrodes [49]. This so-called electrothermal flow is a consequence of the interactions between the applied AC electric field and the Joule heating-induced gradients of fluid conductivity and permittivity [50, 51]. Its magnitude is proportional to the fourth power of the local electric field. Electrothermal fluid circulations can also take place in AC electro-wetting when the frequency of the applied electric field is much greater than the typical frequency of electrode polarization [52,53]. They have been recently demonstrated to enhance microfluidic mixing [54] and immunoassays [45] and to pump bio-fluids [46,47] as well.

To date, however, very little work has been done on Joule heating and its effects on electroosmotic flow in iDEP devices. Sabounchi et al. [58] characterized their iDEP polymeric devices using thermometry experiments and numerical modeling. They observed that Joule heating creates an asymmetric temperature distribution which disturbs the distribution of electric field and electrokinetic forces. Very recently, Hawkins and Kirby [59] developed a numerical model to simulate the electrothermal flow in a two-dimensional constriction in channel depth under DC-offset AC electric fields. They found that fluid circulations may occur in the constriction region at appropriate conditions. It

was also predicted that the electrothermal flow effects serve to enhance particle deflection and trapping in almost all cases. This work presents the first experimental demonstration of electrothermal flow circulations in iDEP devices that are best represented by a constriction microchannel. A numerical modeling of the coupled electric, heat and fluid transport phenomena is developed in order to understand the process and simulate the observed electroosmotic flow patterns in the experiment.

2.2 Experimental setup

The microchannel was fabricated in polydimethylsiloxane (PDMS) using the standard soft lithography technique. It was bonded to a regular glass slide after air plasma treating (PDC-32G, Harrick Scientific, Ossining, NY). The detailed procedure was provided in Ref. [35]. As shown in Fig. 2-1, the channel is 1 cm long with a 200 μm-length constriction in the middle. The widths of the channel and constriction are 400 μm and 40 μm, respectively. The channel is uniformly 40 μm deep. The electric field was supplied by a function generator (33220A, Agilent Technologies, Santa Clara, CA) in conjunction with a high-voltage amplifier (609E-6, Trek, Medina, NY). Fluorescent polystyrene microspheres of 590 nm in diameter (Bangs Laboratories, USA) were used to visualize the flow pattern. They were suspended in 5 mM phosphate buffer with a measured electric conductivity of 470 μS/m at room temperature. Particle motion was monitored using an inverted microscope (Nikon Eclipse TE2000U, Nikon Instruments, Lewisville, TX), through which videos and images were recorded

using a CCD camera (Nikon DS-Qi1Mc). The captured digital videos and images were processed using the Nikon imaging software (NIS-Elements AR 2.30). Pressure-driven flow was eliminated by carefully balancing the liquid heights in the two reservoirs prior to every experiment.

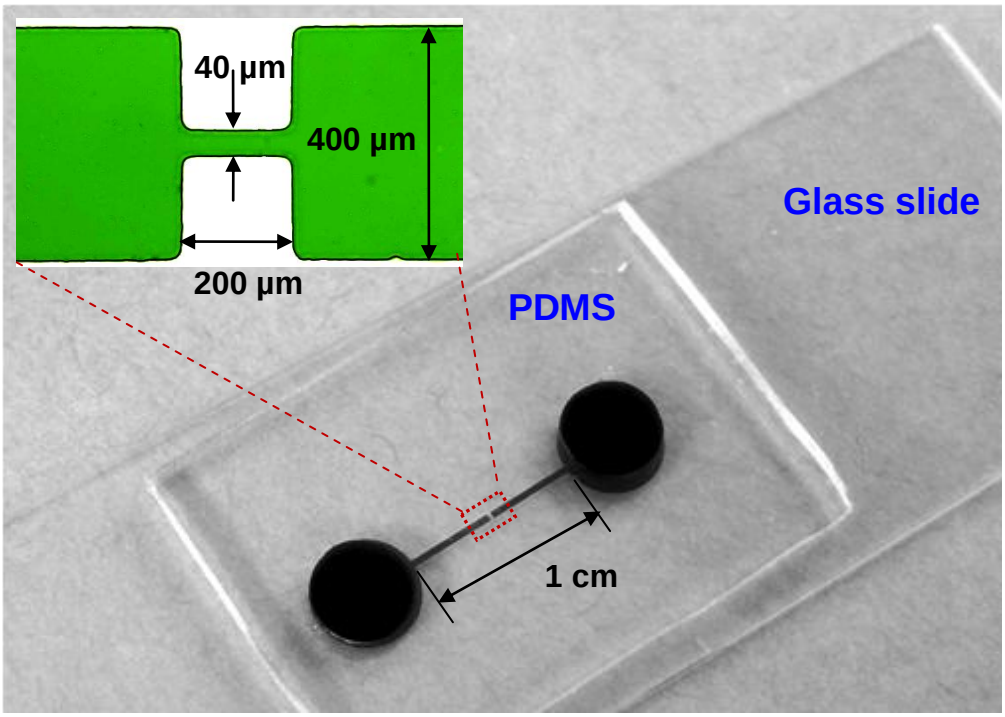

Fig. 2-1: Picture of the constriction microchannel with dimensions labeled in the inset.

2.3 Theory

This section first presents the governing equations for the coupled electric, heat and fluid transport phenomena that typically take place in iDEP devices. Next, the computational domain is determined for the constriction microchannel under investigation. The necessary boundary conditions for solving the governing

equations in this domain are then summarized. Finally, the numerical method is presented along with the material properties that are needed in the modeling.

2.3.1 Electrical equation

With the assumption of non-conducting PDMS and glass substrates, the applied electric field, **E**, is confined within the fluid and is governed by the following two equations [50],

$$\nabla \bullet (\varepsilon \mathbf{E}) = \rho_e \tag{8}$$

$$\nabla \bullet (\sigma \mathbf{E}) + \frac{\partial \rho_e}{\partial t} = 0 \tag{9}$$

Where ε is the permittivity of the fluid, ρ_e is the free charge density, σ is the electrical conductivity of the fluid, and t is the time coordinate. Note that the convection current has been assumed negligible as compared to the conduction current, $\sigma\mathbf{E}$, in Eq. (9). Combining equations (8) and (9) gives rise to a quasi-electrostatic equation for the electric potential [50], ϕ,

$$\nabla \bullet \left[(\sigma + i\omega\varepsilon) \nabla \phi \right] = 0 \tag{10}$$

Where $\omega = 2\pi f$ is the angular frequency of the electric field with f being the ordinary frequency, and $\mathbf{E} = -\nabla\phi$. It is important to note that Eq. (10) is only applicable to a sinusoidally varying potential with a single frequency. For DC fields and AC fields with $f << \sigma/2\pi\varepsilon$ (typically on the order of MHz [45, 47, 51]), Eq. (3) reduces to

$$\nabla \bullet \left(\sigma \nabla \phi \right) = 0 \tag{11}$$

2.3.2 Energy equation

The application of electric field induces Joule heating within the fluid, which, however, extends to both the PDMS and the glass substrates through thermal diffusion in all three dimensions [60]. This significantly complicates the thermal modeling. Therefore thermal analysis is restricted to the fluid phase, and moreover, considered only the heat conduction and convection in the horizontal plane. The real three-dimensional heat transfer conditions surrounding the fluid are approximately simulated by a uniform heat convection boundary condition on the channel wall. This simplified 2D model is sufficient to capture the main feature of electroosmotic flow that was observed in the experiments as demonstrated in the Results section. The steady-state temperature field, T, in the fluid is governed by the following energy equation,

$$\rho C_p \left(\mathbf{u} \bullet \nabla T \right) = \nabla \bullet \left(k \nabla T \right) + \sigma \left\langle \mathbf{E}^2 \right\rangle \tag{12}$$

where ρ is the fluid density, C_p is the specific heat capacity of the fluid, **u** is the fluid velocity, k is the thermal conductivity of the fluid, and the last term represents the time-averaged Joule heating. Note that the convective term on the left-hand-side of Eq. (12) may not be neglected because the thermal Peclet number (i.e., the ratio of the rate of heat convection to that of heat diffusion) can easily reach the order of 1 in the experiments.

2.3.3 Flow field equation

The steady-state flow field of the fluid is governed by the Navier-Stokes equation along with the continuity equation [50],

$$\rho \mathbf{u} \bullet \nabla \mathbf{u} = -\nabla p + \nabla \bullet \left(\eta \nabla \mathbf{u} \right) + \left\langle \mathbf{f}_e \right\rangle \tag{13}$$

$$\nabla \bullet \mathbf{u} = 0 \tag{14}$$

Where p is the pressure, η is the dynamic viscosity of the fluid, and $\langle \mathbf{f}_e \rangle$ is the time-averaged electrical body force or the so-called electrothermal force [40]. The general form of $\langle \mathbf{f}_e \rangle$ is given as [61],

$$\left\langle \mathbf{f}_e \right\rangle = \left\langle \rho_e \mathbf{E} - 0.5 \mathbf{E}^2 \nabla \varepsilon \right\rangle \tag{15}$$

Where, the first and second term on the right-hand-side represents the Coulomb force and dielectric force, respectively. Replacing the free charge density, ρ_e, in Eq. (8), rewrites Eq. (15) as [62]

$$\left\langle \mathbf{f}_e \right\rangle = \left\langle \left(\varepsilon \nabla \bullet \mathbf{E} + \alpha \varepsilon_0 \mathbf{E} \bullet \nabla T \right) \mathbf{E} - 0.5 \alpha \varepsilon_0 \mathbf{E}^2 \nabla T \right\rangle \tag{16}$$

Where α is the linear temperature coefficient of fluid permittivity, i.e., $\varepsilon/\varepsilon_0 = 1+\alpha(T-T_0)$ with ε_0 being the fluid permittivity at the reference temperature T_0. Therefore, it is the interaction of electric field with Joule heating-induced temperature gradients that generates the volume electrothermal force.

2.4 Numerical method and boundary conditions

As noted earlier, only the fluid phase is considered in the numerical model and solved for the coupled electric potential, temperature, and flow fields in two-dimension for simplicity. Due to the symmetry with respect to the channel centerline, the computational domain comprises one half of the entire microchannel in the horizontal plane. Fig. 2-2 shows the close-up view of the meshed constriction region, where the meshing parameters will be explained in the flowing paragraph. To solve for the coupled electric, energy, and fluid equations, four sets of boundary conditions are imposed to the inlet, outlet, channel wall, and channel symmetry, respectively, as highlighted in Fig. 2. These boundary conditions except the symmetric ones are summarized below.

Numerical simulation was carried out using COMSOL 3.5a multiphysics software (Burlington, MA). The Conductive Media DC, Convection and Conduction, and Incompressible Navier-Stokes modules were used to solve for the coupled electric potential, temperature, and flow fields. The Convection and Conduction module was chosen from the COMSOL Multiphysics application mode. The Conductive Media DC and Incompressible Navier-Stokes modules were selected from the MEMS application mode. The 2D geometry of one half of the entire microchannel was created using the drawing tools in COMSOL. The geometry was then meshed with triangular meshes using the free mesh parameters tool box. The boundaries are more densely meshed with the maximum element size of 5 μm, and the whole domain contains a total of around

100,000 elements. The constriction region consists of more mesh elements than the rest of the channel. Model validation was done by increasing the number of mesh elements ranging from 5,000 to 200,000. There was no noticeable change in the results when the number of mesh elements was beyond 50,000. In addition, as COMSOL can only handle pure DC or pure AC electric fields, we have to modify the governing equations to accommodate DC-biased AC electric fields that were used in the experiment.

2.4.1 Conductive media DC

Inlet: $\phi = V_0$, where V_0 is the applied electric potential.

Outlet: $\phi = 0$, i.e., grounded.

Channel wall: $\mathbf{n} \bullet (\sigma \nabla \phi) = 0$, i.e., electrically insulating, where **n** denotes the unit normal vector.

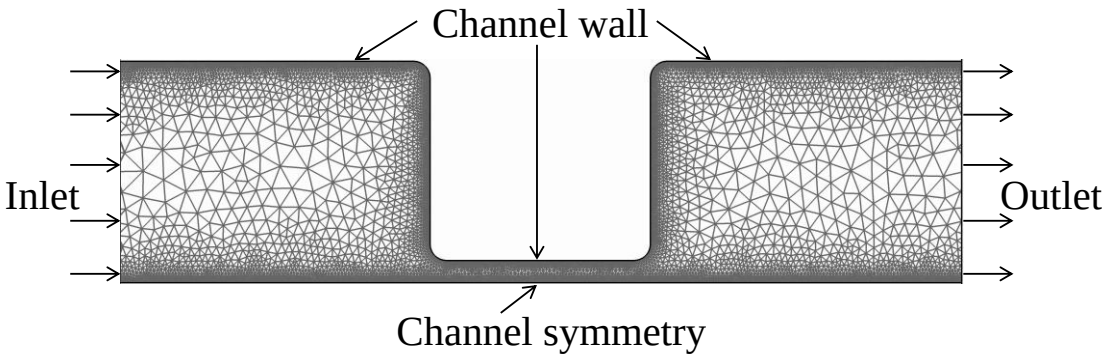

Fig. 2-2: Zoom-in top view of the meshed constriction region of the microchannel. Note that the computational domain comprises one half of the entire microchannel.

2.4.2 Convection and Conduction

Inlet and outlet: $T = T_0$, i.e., the fluids in the end-channel reservoirs are assumed isothermal as their volumes are much larger than the fluid within the microchannel [59, 63].

Channel wall: $q'' = -h(T - T_0)$, where q'' is the outward heat flux due to heat convection with an assumed heat transfer coefficient h. The magnitude of h is determined by matching the model predicted rise in electric current with the experimentally measured data. This value is assumed constant throughout the channel wall and independent of the fluid temperature for simplicity.

2.4.3 Incompressible Navier-Stokes

Inlet and outlet: $\mathbf{n}\bullet(\eta\nabla\mathbf{u}) = 0$ and $p = 0$, i.e., the fluids in the end-channel reservoirs are assumed to have zero viscous stress and zero pressure (open to the air).

Channel wall: $\mathbf{u} = \varepsilon\zeta\nabla\phi_{DC}/\eta$, where ζ is the zeta potential of the channel wall. This is a well-accepted slip boundary condition for electroosmotic flow in microchannels with thin electric double layers (approximately 5 nm for the buffer solution used in this work) [62]. It is important to note that only the DC component of the applied voltage drop, ϕ_{DC}, can drive electroosmotic flow. However, both the DC and AC components generate Joule heating and contribute to electrothermal flow via the electrothermal force, $\langle\mathbf{f}_e\rangle$ in Eq. (16). This indicates that the relative strength of electroosmotic flow and electrothermal flow

can be varied by adjusting the DC to AC field ratio, which will be demonstrated in the results section.

2.4.4 Temperature dependent properties

Temperature is the coupling parameter in solving the electrical, energy and fluid equations as it affects the fluid properties. We considered the temperature dependence of fluid permittivity, electric conductivity and viscosity using the following expressions [41]:

$$\varepsilon(T) = \varepsilon_0\left[1+\alpha\left(T-T_0\right)\right] \tag{10}$$

$$\sigma(T) = \sigma_0\left[1+\beta\left(T-T_0\right)\right] \tag{11}$$

$$\eta(T) = 2.761\times10^{-6}\exp(1713/T) \tag{12}$$

Where σ_0 is the electric conductivity of the fluid at the reference temperature, and β is its linear temperature coefficient. The values of the constants and fluid properties involved in the numerical simulation are listed in Table 1.

Name	Value	Unit	Description
T_0	293	K	Reference temperature
ε_0	7.10e-10	F/m	Fluid permittivity at T_0
α	−0.0046	1/K	Temperature coefficient of fluid permittivity
σ_0	0.047	S/m	Fluid electric conductivity at T_0
β	0.02	1/K	Temperature coefficient of fluid electric conductivity

ρ	1000	kg/m^3	Fluid density
C_p	4.186	kJ/(kg·K)	Fluid heat capacity
K	0.6	W/(m·K)	Fluid thermal conductivity
ζ	−0.05	V	Wall zeta potential
H	20×10^3	$W/(m^2\cdot K)$	Convective heat transfer coefficient

Table 2-1: List of constants used in the numerical simulation of Joule heating effects on electroosmotic fluid flow [64].

The convective heat transfer coefficient, h, was determined by matching the model predicted rise in electric current density with the experimentally measured increase in electric current. In the experiment the electric current was noticed to increase from the initial 52 μA (i.e., at the room temperature) to the quasi-steady 66 μA three minutes after a 600 V voltage drop (either DC or AC) was applied across the constriction microchannel. In COMSOL, an initial value of h was first assumed to start the 2D simulation. The electric current density was read directly from the predefined quantity in COMSOL, Total current density, at a position that was near the outlet of the microchannel. Its rise due to Joule heating was determined by comparing the electric current densities at the same position of the microchannel when Joule heating is absent and present, respectively. Thus obtained value was then compared with the experimentally measured increase in electric current (which is about 27%). If not match, a new value of h was assigned to repeat the above steps.

Using this iteration method, it was found that the assumption of h = 20×10^3 W/(m^2·K) (see Table 2-1) yielded the closest match with the experimental data. This h value is recognized to be much larger than that reported in Ref. [49] and those used in other studies [60,66,67] as well, which indicates that Joule heating of the fluid was actually dissipated mainly from the bottom glass slide in our microchannel. It is because glass has a much higher thermal conductivity than PDMS [60,66,67], and also the glass slide was sitting on the large microscope working stage in the experiment. In spite of this discrepancy, the developed 2D model is still sufficient to capture the main feature of the observed electroosmotic flow patterns in the experiments, which will be presented in the results section.

2.5 Results and discussion

Fig.2-3 shows the comparison of the experimentally obtained pathlines of 590 nm particles (bottom) and numerically predicted streamlines (top) of electroosmotic flow through the microchannel constriction under various DC-biased AC voltages. The total RMS magnitude of the applied DC and AC voltages was fixed at 600 V, yielding an average electric field of about 600 V/cm over the channel length. The frequency of the AC voltages was fixed at 1 kHz. There was no noticeable change in the flow pattern when the AC frequency was varied from 500 Hz to 10 kHz (the maximum frequency that our amplifier actually allows is less than 15 kHz). At frequencies lower than 200 Hz, the AC electrophoretic motion of particles was observed to blur the particles, which

significantly affects the flow visualization. In addition, the flow patterns in all cases presented below formed quickly after the voltage was supplied and appeared to achieve steady state within seconds.

2.5.1 Effect of DC biased AC voltages

Under a 600 V DC voltage, there are no apparent disturbances to both the observed pathlines (bottom) and the predicted streamlines (top) in Fig. 2-3(a) as compared to previously reported electroosmotic flow profiles in the presence of Joule heating [60,65,66]. However, when the DC voltage was decreased to 100 V and meanwhile a 500 V AC voltage was applied to maintain the total magnitude, a pair of small counter-rotating circulations was observed to occur at the downstream end of the constriction in Fig. 2-3(b). This phenomenon, as also predicted by the numerical modeling, indicates that the electrothermal flow induced in the constriction starts to become comparable to the reduced electroosmotic flow under a lowered DC voltage. The electrothermal fluid circulations appear to obstruct the electroosmotic flow in the channel center while enhancing it near the corners of the constriction. It was also noticed in Fig. 2-3(b) (bottom image) that the fluorescent particles covered a narrower region at the downstream side of the constriction than at the upstream side. This is believed to be a consequence of the constriction-induced dielectrophoretic focusing effect on 590 nm particles [35].

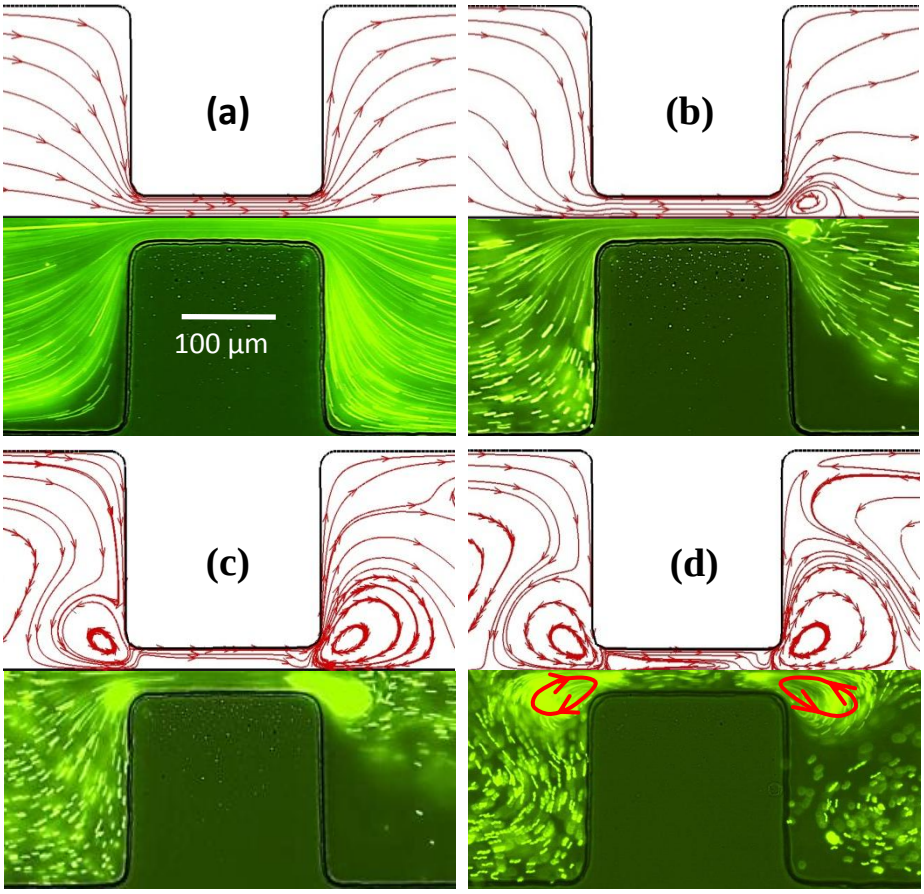

Fig. 2-3: Comparison of simulation (top) and experimental (bottom) results of electroosmotic flow patterns in the microchannel constriction region under various DC-biased AC (fixed at 1 kHz) voltages: (a) 600 V DC, (b) 100 V DC/500 V AC, (c) 50 V DC/550 V AC, and (d) 20 V DC/580 V AC. The average electric field is about 600 V/cm over the channel length. The Joule heating-induced electrothermal flow circulations were observed to start occurring at the downstream end of the constriction under 100 V DC/500 V AC, see panel (b). The flow direction is from left to right in all cases. The arrowed loops in the experimental image of (d) indicate the directions of the electrothermal flow circulations.

Similar to those previously studied in eDEP [44-57], electrothermal flows in iDEP devices also arise from the action of electric field (both DC and AC) to the fluid inhomogeneities (predominantly electrical properties including conductivity and permittivity) formed in the constriction region due to Joule

heating-induced temperature gradients. Fig. 2-4 shows the numerically predicted temperature and electric field contours in the constriction region at 100 V DC/500 V AC. As expected, the fluid temperature within the constriction is much higher than that outside it because the electric field is locally amplified by the constriction. Moreover, the axial temperature distribution is not exactly symmetric about the constriction, and actually shifts slightly downstream due to the electroosmotic fluid advection, i.e., the convective term on the left-hand-side of Eq. (12). This effect is more pronounced in the 500 V DC case, and seems consistent with the temperature distribution in capillary or microchip-based electrophoresis where the Joule heating-caused high temperature plateau in the main body of the capillary or microchannel was found to shift toward the outlet reservoir due to electroosmotic effect [65,66].

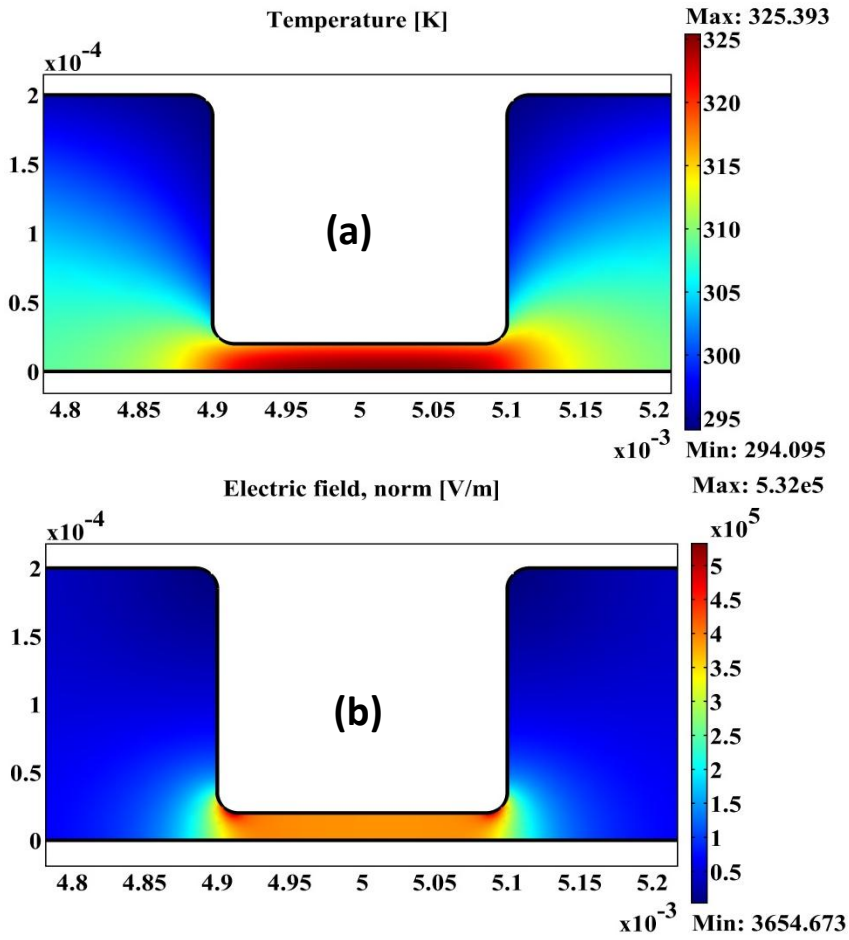

Fig. 2-4: Illustration of the contours of fluid temperature (a) and electric field (b) in the microchannel constriction. The applied voltages are 100 V DC and 500 V AC. The fluid reaches a high temperature within the constriction due to the locally amplified electric field, which is shifted slightly downstream due to electroosmotic flow. The flow direction is from left to right.

Further decreasing the DC voltage to 50 V while increasing the AC voltage to 550 V, we observed electrothermal fluid circulations at both the downstream and the upstream ends of the channel constriction as demonstrated in Fig. 2-3(c). However, the downstream circulations appeared to be larger in size than the upstream pair, which is also reasonably captured in the numerical modeling. Moreover, the upstream circulations were noticed to rotate in the mirror direction

of the downstream ones. That is to say, the electrothermal body force, $\langle \mathbf{f}_e \rangle$, tends to slow down the incoming fluid near the corners at the upstream end of the constriction, and then pull it to the channel center where the local electroosmotic fluid flow is enhanced by the electrothermal flow. Upon decreasing the DC voltage to 20 V while increasing the AC voltage to 580 V, all circulations were observed to grow even larger in size, and the electrothermal flow seemed to dominate the electroosmotic flow in the constriction region. However, the upstream circulations are still a little smaller than the downstream ones due to the electroosmotic flow, which agree qualitatively with the numerical modeling as demonstrated in Fig. 2-3(d). It is noted that similar fluid circulations have been numerical predicted by Hawkins and Kirby [59] in a recent paper, where the electrothermal body force was considered for the first time in studying Joule heating effects on electrokinetic flows. In addition, several other similar studies on Joule heating in electrokinetic microchannel chips have been reported [42,55,58,60,66,67], which, however, all ignored the Joule heating-induced electrothermal flow.

It was found that the induced dielectrophoretic velocity of the 590 nm [30,35] tracing particles was on the order of 50 μm/s in the fluid circulation regions, and could reach 150 μm/s if the particle was within 2 μm distance from the corners of the constriction. Accordingly, the predicted electroosmotic fluid velocity varied approximately from 300 μm/s to 450 μm/s for the 20 V DC/580 V AC case, at which the electroosmotic flow was the weakest among the four

cases shown in Fig. 2-3. We also attempted to track the particle rotation speed within the circulations, which is hard due to the strong fluid circulations and the limited frame speed of our camera (about 12 frames per second). However, it is certain that the measured particle speed is over 1000 μm/s. Therefore, the Joule heating-induced electrothermal flow should dominate the particle motion in the 20 V DC/580 V AC case. For other cases in Fig. 2-3 with higher DC voltages, the electroosmotic flow itself should be already large enough to dominate the particle motion. Therefore, the induced dielectrophoresis of tracing particles should not affect significantly the particle trajectories. Namely, the observed particle pathlines can be used to compare with the numerically predicted fluid streamlines.

2.5.2 Effect of AC voltages

Under a 600 V pure AC voltage, there is no net electroosmotic flow in the microchannel. Therefore, the electrothermal fluid circulations should become symmetric about the constriction, which is clearly demonstrated in both the experiment (left plot) and the modeling (right plot, the background shows the fluid velocity contour and the lines represent fluid streamlines) in Fig. 2-5(c). The same figure also shows the electrothermal flow patterns under 200 V (a), 400 V (b), and 800 V (d) pure AC voltages. In Fig. 5(a) fluid circulations are barely seen because the applied 200 V/cm electric field is too low to cause sufficient temperature gradients for electrothermal flows. As a matter of fact, the largest rise in fluid temperature under 200 V AC is less than 5 K at the center of the

constriction as shown in Fig. 2-6. Increasing the AC voltage rapidly elevates the fluid temperature as Joule heating is proportional to the electric field squared, which is illustrated by the axial fluid temperature profiles along the channel centerline in Fig. 2-6. Consequently, increasing the AC voltage should dramatically enhance the electrothermal flow in the constriction region as the electrothermal force scales with the fourth power of electric field. This is justified by our experimental and simulation results in Fig. 2-5.

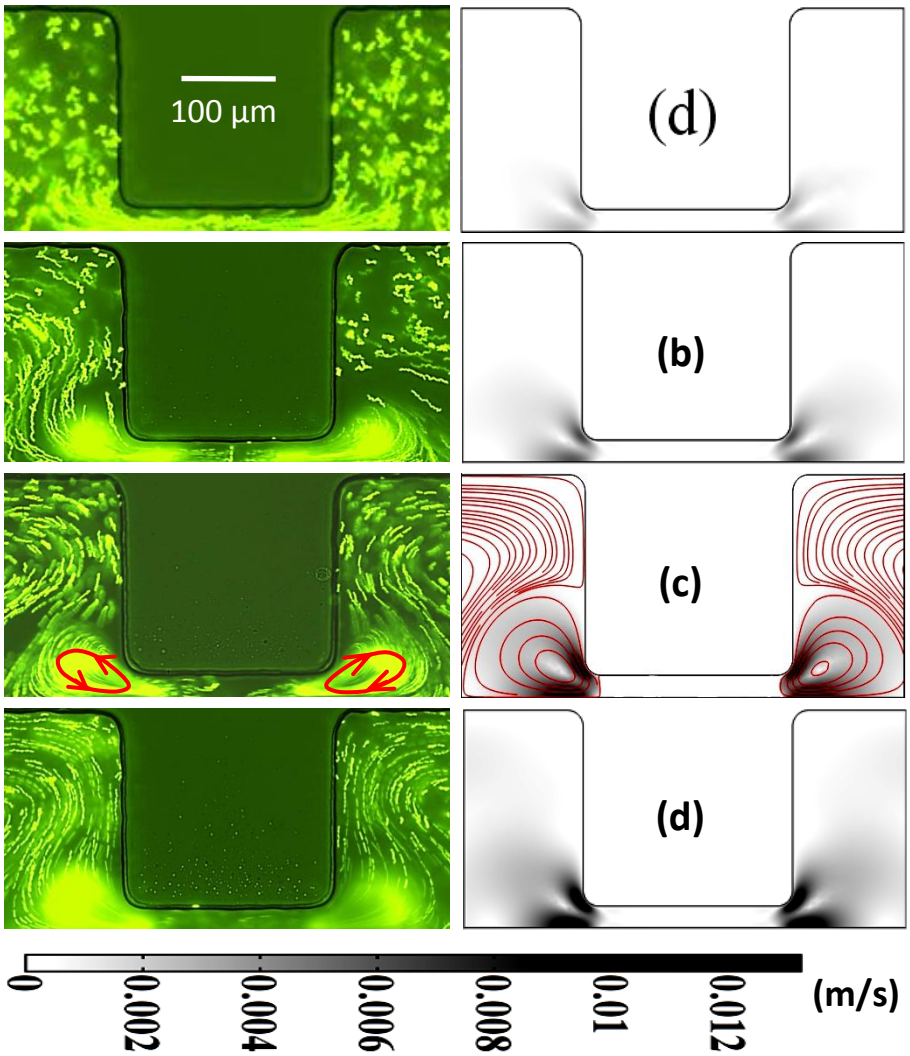

Fig. 2-5: Comparison of simulation (right column, background shows the contour of fluid velocity) and experimental (left column) results of electroosmotic flow in the microchannel constriction region under various pure AC voltages (fixed at 1 kHz): (a) 200 V, (b) 400 V, (c) 600 V, and (d) 800 V. The simulation result in panel (c) also includes the fluid streamlines, whose directions are shown in Fig. 3. There is no net flow in the main channel. The arrowed loops in the experimental image of (c) indicate the directions of the electrothermal flow circulations.

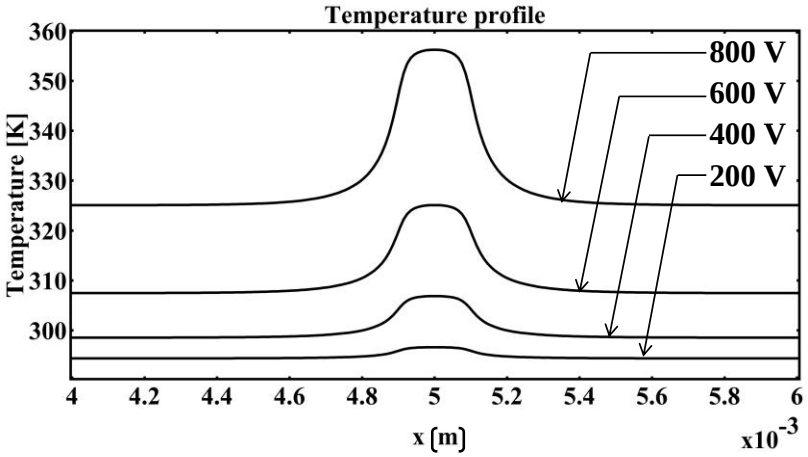

Fig. 2-6: Comparison of the axial fluid temperature profiles along the centerline of the constriction microchannel under pure AC voltages ranging from 200 to 800 V. All profiles are symmetric about the constriction as there is no net electroosmotic flow in the channel.

2.5.3 Effect of constriction size

This section presents the numerical prediction of the Joule heating effects on the size of the constriction. Fig. 2-7 shows the temperature distribution plot for 20 and 80 µm width of the constriction for a ratio of 50 V DC and 550 V AC. Since Joule heating is proportional to the square of electric field, the larger constriction width will have low electric field when compared to smaller constriction width. Consequently temperature is higher in smaller width and lower in larger constriction width as joule heating depends on the locally amplified electric field. The temperature reaches to a maximum of 319 K for 80 µm constriction width as the electric field strength is less due to increased constriction area whereas in 20 µm constriction width maximum temperature reaches around 330 K. The plots shown are symmetric about the constriction.

Similarly a comparative study was performed on the electroosmotic velocity of the fluid. Fig. 2-8 compares the velocity field streamline plot of 20, 40 and 80 µm constriction widths for a ratio of 50 V DC and 550 V AC. It was observed that the velocity in the 20µm depth constriction was larger when compared to the other constriction width. As the temperature increases fluid viscosity decreases which in turn increases the electroosmotic velocity. The mentioned ratio was taken to account for both electrothermal flow as well as electroosmotic flow. The circulations seen in the upstream and downstream end are due to the electrothermal force caused due to the joule heating induced temperature gradients in the fluid properties. The colored lines shown in the plot corresponding to the legend illustrates the velocity magnitude. The maximum velocity always occurs in the corner of the constriction because electric field is highest in that region and so the temperature gradients. As illustrated the velocity highest for the 20 micron constriction width and gradually reduces for other two cases.

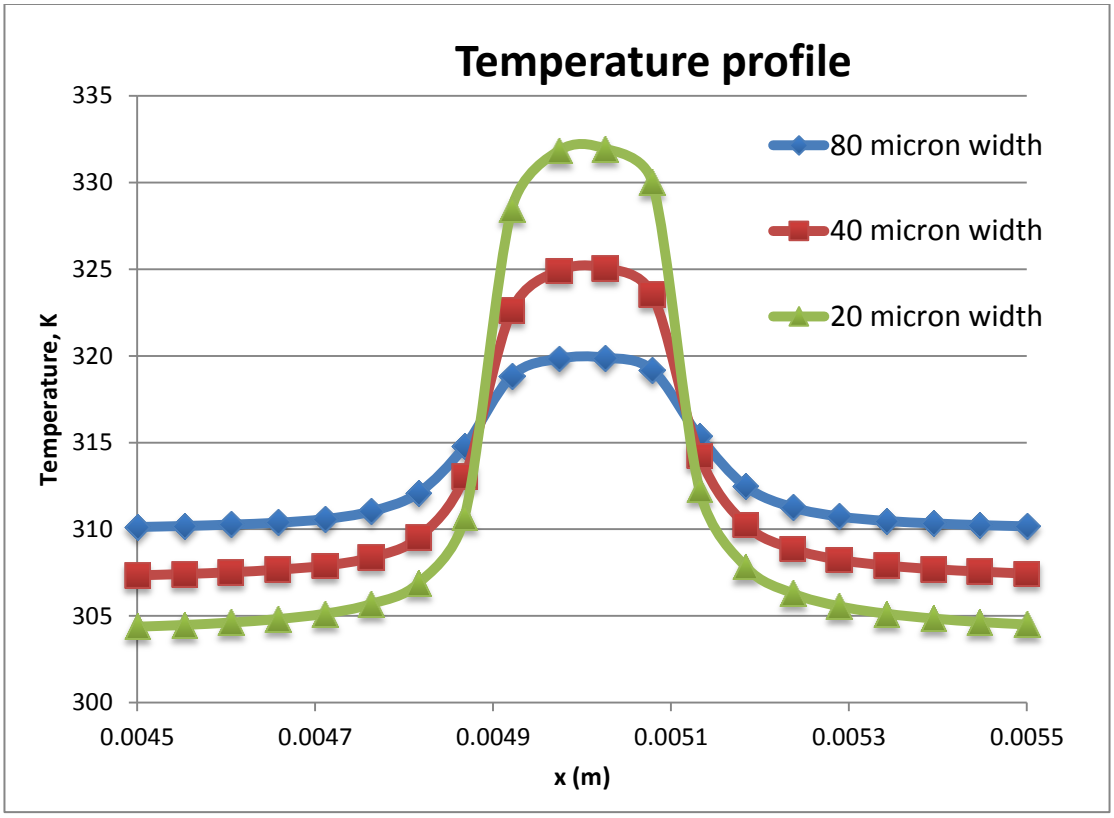

Fig. 2-7: Comparison of the axial fluid temperature profiles along the centerline for constriction widths of 80 μm and 20 μm under voltage of 50 V DC 550 V AC.

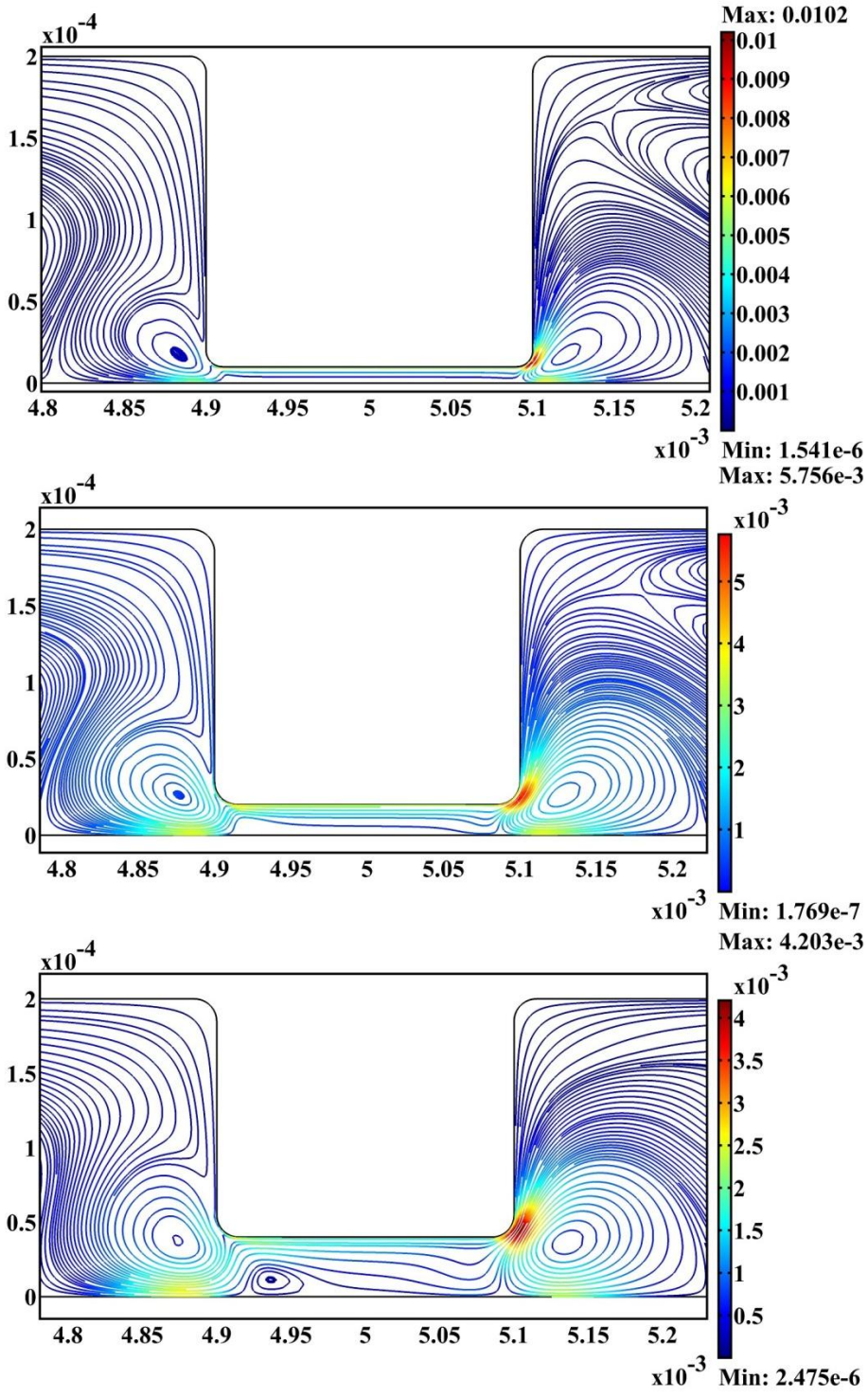

Fig. 2-8: Comparison of velocity field streamlines for constriction sizes of 80 µm, 40 µm and 20 µm under voltages of 50 V DC 550 VAC. Legends in the figure indicates the magnitude of velocity at specified locations.

2.6 Summary

A combined experimental and numerical study of Joule heating effects on electroosmotic flow in a typical iDEP device has been performed. Fluid circulations were observed around the constriction for the first time using small fluorescent tracing particles. They are formed through a mechanism identical to the traditional AC electrothermal flow in eDEP devices, which, as verified by the numerical modeling, is attributed to the interaction between the applied electric field and the fluid inhomogeneities in the constriction region due to Joule heating-induced temperature gradients. Through both experimentation and simulation, it has been examined how the DC (in DC-biased AC fields) and AC (in pure AC fields) voltages may alter the electroosmotic flow pattern in the constriction microchannel. It is found that the electrothermal fluid circulations grow in size and speed dramatically with the increasing AC voltage in both cases. Such Joule heating-induced electrothermal flow circulations should be taken into account in the design and operation of iDEP devices, especially when highly conductive solutions and/or large electric fields must be employed. They may potentially be harnessed to enhance microfluidic mixing and immunoassay for lab-on-a-chip applications.

CHAPTER 3

JOULE HEATING EFFECTS ON ELECTROKINETIC PARTICLE TRANSPORT IN CONSTRICTION MICROCHANNELS

3.1 Introduction

Lab-on-a-chip devices have been increasingly used in the biomedical applications for the manipulation of biological cells and particles. One of the important applications is the focusing of particles into single stream. It can be achieved through various principles like magnetophoresis [69], dielectrophoresis (DEP) [71], acoustic means [70] and Optical phenomena [68]. DEP is one of the highly used methods in manipulation of particles and cells in a microchannel. Dielectrophoresis is the force exerted on the dielectric particle through the application of non-uniform electric field generated by either micro electrodes or in-channel hurdles in the microchannel. The strength of DEP force depends on size, electrical properties of the medium and particles and frequency of the applied electric field.

Focusing is achieved by both electrode [15,16] and insulator based dielectrophoresis [17-19]. In the former method microelectrodes are placed in desired places in the microchannel to generate spatially non-uniform electric field. In the latter method insulating structure or hurdles placed in the channel generate spatially non-uniform electric field through remote electrodes [28-37].

However the particles in iDEP devices experience Joule heating in the regions of locally amplified electric field that affect the cell viability and the throughput.

Recently zhu and xuan [35] presented a fundamental study of focusing in a single microchannel constriction without the effect of joule heating. It's been found that better focusing is implemented under DC biased AC voltages (10 KV/m) than at pure DC electric fields (100 kV/m). Jen and Huang [72] presented a study on design of an insulator-based dielectrophoretic micro device with effective focusing of biological cells. The cells are, therefore, repelled toward the center of the microchannel by the negative dielectrophoretic forces generated by the insulating structures. It was found that decreasing inlet velocity increases the efficiency of focusing because the higher velocity results in more lateral expansion. Also, Hawkins and Kirby [59] performed a parametric study on particle deflection and tapping in a constriction based microchannel. Electrothermal effects perturb the electroosmotic flow field, creating vortices near the channel constriction and enhancing the deflection and trapping effects. ET effects alter particle deflection and trapping responses in insulator-based dielectrophoresis devices, especially at intermediate device aspect ratios and in solutions of higher conductivity. The impact of ET effects on particle deflection and trapping are diminished when particle electrophoretic mobility or channel electroosmotic mobility is high.

This work presents the systematic study of electrothermal effects on electrokinetic particle motion in 15 and 45 μm depth microchannel constrictions

under DC and DC biased AC electric fields. A numerical model is developed to capture the particle trace observed in the experiments.

3.2 Experimental setup

The microchannel was fabricated in Polydimethylsiloxane (PDMS) using the standard soft lithography technique. It was bonded to a regular glass slide after air plasma treating (PDC-32G, Harrick Scientific, Ossining, NY). The detailed procedure is referred to Zhu and Xuan [35]. As shown in Figure 2-1, both the channels are 1 cm long and 400 μm wide with a constriction length of 200 μm in the middle. The two channels are uniformly 45 μm and 15 μm deep with a constriction width of 45 μm and 38 μm respectively. The electric field was supplied by a function generator (33220A, Agilent Technologies, Santa Clara, CA) in conjunction with a high-voltage amplifier (609E-6, Trek, Medina, NY). Polystyrene particles of 3 μm in diameter (Bangs Laboratories, USA) were used to visualize the flow pattern. They were suspended in 5 mM phosphate buffer with a measured electric conductivity of 0.05 S/m at room temperature. Particle motion was monitored using an inverted microscope (Nikon Eclipse TE2000U, Nikon Instruments, Lewisville, TX), through which videos and images were recorded using a CCD camera (Nikon DS-Qi1Mc). The captured digital videos and images were processed using the Nikon imaging software (NIS-Elements AR 2.30). Pressure-driven flow was eliminated by carefully balancing the liquid heights in the two reservoirs prior to every experiment.

3.3 Theory

The governing equations for the coupled electric, heat and fluid flow which are responsible for the electrokinetic transport phenomena have been previously explained in the theory section of chapter 2. The following paragraph presents the governing equation for the dielectrophoretic force and velocity which is responsible for the transverse movement of the particles in non-uniform electric field.

3.3.1 Dielectrophoretic force

Dielectrophoresis refers to the response of an electrically polarized object (either charged or non-charged) in a non-uniform electric field. Consider a spherical, uncharged, uniform, ideal dielectric particle with a finite polarizability, suspended in empty space. If a uniform electrical field is applied to this system, the sphere polarizes and there is a net positive charge at one end of the sphere and a net negative charge on the other end of the sphere. Coulomb forces on either end of the sphere are equal and opposite, and the net Coulomb force is zero. If the electric field is non-uniform, however, the side of the sphere with the larger electric field feels a larger attractive force, and the net force moves the particle toward the region of high electric field. This motion toward high electric field regions is termed as positive dielectrophoresis [3].

For a particle suspended in a medium, the net force on the particle is dependent on the difference between the polarization of the particle and the polarization of the medium. If the medium polarizes less than the particle, the

particle experiences positive dielectrophoresis and moves toward the high electric field region. If the medium polarizes more than the particle, the particle experiences negative dielectrophoresis and moves toward the low electric field region. In both cases, the direction of motion of the particle is a function of the electric field magnitude, but not its polarity. Thus the dielectrophoretic motion of an uncharged, uniform, ideal dielectric object in an ideal dielectric medium is independent of whether a DC or AC field is used, or even the frequency of the field, as long as the permittivity is independent of frequency.

As the electric field becomes non-uniform, particles experience variable dielectrophoretic forces, $\mathbf{F}_{DEP}$, when they move electrokinetically through the constriction. Using the dipole moment approximation, $\mathbf{F}_{DEP}$ on an isolated spherical particle in DC fields is given by [35]

$$F_{DEP} = \pi\varepsilon(T)a^3 f_{CM}(E \bullet \nabla E) \tag{17}$$

$$f_{CM} = (\sigma_p - \sigma_f)/(\sigma_p + 2\sigma_f) \tag{18}$$

Where $\varepsilon(T)$ is the fluid permittivity, a is the radius of the particle, f_{CM} is the Clausius-Mossotti (CM) factor, **E** is electric field strength, σ_p the electric conductivity of particles, and σ_f the electric conductivity of the medium. It is important to note that Eq. (17) is valid only when the particle size is much smaller than the characteristic length scale of the electric field [46]. Apparently, this condition may break down when particles approach the constriction. Therefore,

we will introduce a correction factor in the Modeling section to account for the size effects on particle dielectrophoresis.

In DC and low-frequency AC electric fields (<100 kHz), polystyrene particles are less conductive than the medium, i.e., $\sigma_p < \sigma_f$, leading to a negative dielectrophoresis. In other words, $\mathbf{F}_{DEP}$ is directed towards the lower electric field region. By balancing $\mathbf{F}_{DEP}$ with the Stokes drag force, we obtain the dielectrophoretic particle velocity, $\mathbf{U}_{DEP}$, which is then superimposed to electrokinetic flow (a combination of fluid electro-osmosis and particle electrophoresis), $\mathbf{U}_{EK}$, to get the net particle velocity, $\mathbf{U}_p$, i.e.,

$$\mathrm{U_p} = \mathrm{U_{EK}} + \mathrm{U_{DEP}} = \mu_{EK}\mathrm{E} + \mu_{DEP}\left(\mathrm{E} \bullet \nabla \mathrm{E}\right) \tag{19}$$

$$\mu_{DEP} = \varepsilon(T)a^2 \mathrm{f_{CM}} / 6\mu(T) \tag{20}$$

Where, μ_{EK} is the electrokinetic mobility, μ_{DEP} the dielectrophoretic mobility which is negative as $f_{CM} < 0$.

3.4 Numerical modeling

In order to understand the effects of electrothermal force on the particle motion a numerical model was developed to simulate the particle trajectories through the constriction microchannel. It was carried out using COMSOL 3.5a multiphysics software (Burlington, MA). The application modes are chosen the same way as discussed in the chapter 2. The geometry was then meshed with triangular meshes using the free mesh parameters tool box. The domain is finely meshed with 243,000 elements with the maximum element size of 5.5 μm in the

domain. Only the channel domain is considered for the numerical modeling and solved for the coupled electric, temperature, and flow field equations. Due to the symmetry with respect to the channel centerline, the computational domain comprises one half of the entire constriction microchannel in the horizontal plane.

In this model a correction factor was introduced to avoid the under or over estimation of the dielectric force when particles pass through the constriction. As predicted by zhu and Xuan, correction factor increases from 0 to 1 as the particle size decreases. In order to determine the particle velocity, electrokinetic and dielectrophoretic mobility were identified from the experiments and the formula respectively. The electrokinetic mobility was found to be between 0.8e-8 to 1.2e-8 m^2/s. The total particle velocity would be the addition of electrokinetic velocity (includes the electro-osmosis, electrophoresis and electrothermal force) and the dielectrophoretic velocity. This is represented in COMSOL as a subdomain expression and solved along with coupled electric, temperature, and flow field equations.

Name	Value	Unit	Description
h1	20×10^3	$W/(m^2.K)$	Convective heat transfer coefficient for 45 µm depth channel
h2	20×10^5	$W/(m^2.K)$	Convective heat transfer coefficient for 15 µm depth channel
ζ_p	-0.035	V	Particle zeta potential
c	0.8	-	Correction factor
CM	-0.5	-	Claussius-Mosotti factor

a	1.5e-6	m	Radius of the particle

Table 3-1: Shows the list of constants and fluid properties used in the numerical simulation of electrokinetic particle transport.

The convective heat transfer coefficient, *h*, was determined by matching the electric current density obtained from modeling with the experimentally measured increase in electric current as discussed in the chapter 2.

3.5 Results and discussion

3.5.1 Particle motion at various DC voltages

This section presents the parametric study of electric field effects on the motion of 3 µm particles in a constriction based microchannel. Fig. 3-1 and 3-2 compares the results of numerical simulation and experiments for motion of 3 µm diameter particles in a 15 and 45 µm depth microchannels under DC electric fields coupled with Joule heating induced electrothermal flow. The total voltage was varied from 200 V DC to 800 V DC and the frequency was set to 1 kHz and all other parameters are fixed for both the cases. Particle and wall zeta potential was fixed to 35 and 50 mV respectively and temperature dependence of zeta potential on the particles is not considered. In the simulation the correction factor for the particle was taken as 0.8 in order to account for the particle size and interactions on the dielectrophoretic velocity. In this work the particle conductivity is less than that of the conductivity of the medium. According to the phenomenon of negative dielectrophoresis the particle should focus to the center of the channel due to non-uniform electric field from the constriction corners i.e., particles will move towards the region of lower electric field. The focusing

depends upon the strength of the non-uniform electric field developed due to the change in cross sectional area of the channel. Fig. 3-1(a) shows the experimental and numerical images of 3 μm diameter particle motion in a 15 μm depth channel for 200 V DC. As it can be seen the particles are dispersed after exiting the constriction which means there is barely any focusing or electrothermal effect. The locally amplified electric field strength within the constriction is not strong enough to generate high dielectrophoretic force to push the particles to the center of the channel. The numerical prediction seems to agree with the experiments. As the applied voltage is increased particle trajectory can be controlled in a more efficient way.

Fig. 3-1(b) implies that particles begin to travel in a more confined path at a voltage of 400 V DC. As the magnitude of DC electric field increases, particle nearing the upstream end of the constriction will be forced away from the constriction corners by negative DEP. As a result, particles follow small stream width at the large electric fields after exiting the constriction. This is illustrated in the fig. 3-1 (a-d) and the numerical predictions seem to agree well with the experiments which indicate the accuracy of the assumed correction factor. Stream width of the particles exiting the constriction gets reduced for increasing DC magnitudes.

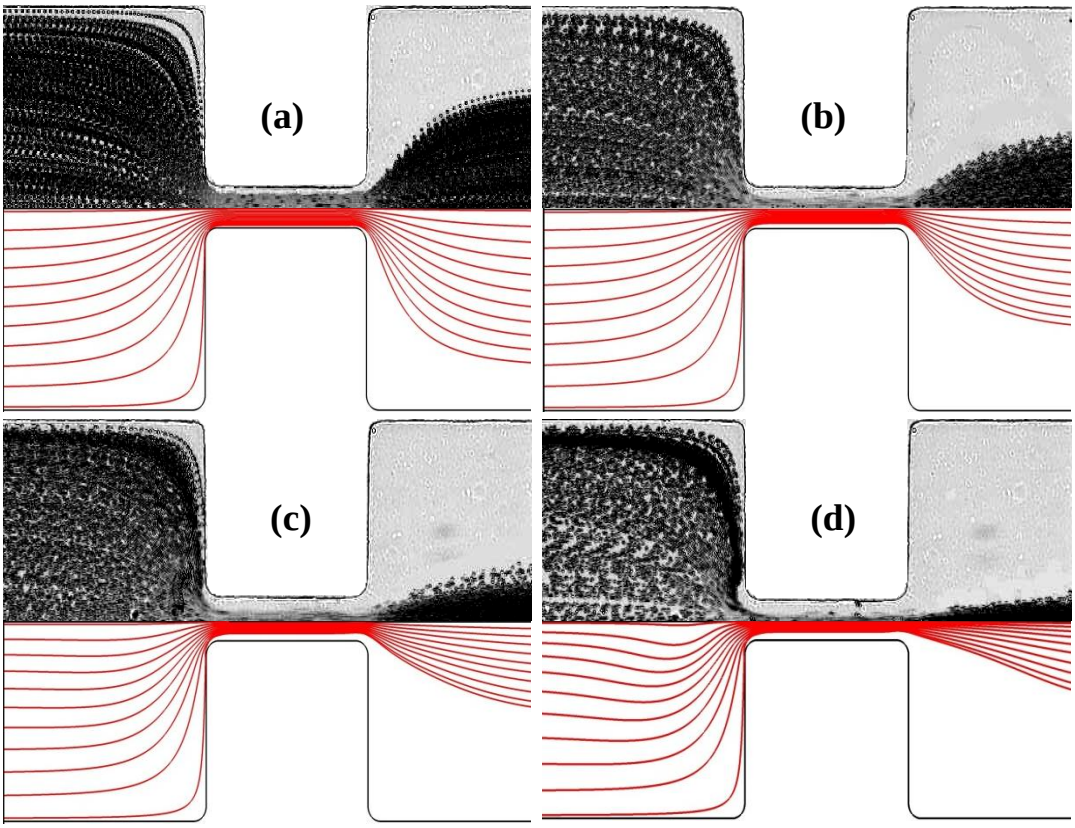

Fig. 3-1: Motion [experiment (top) and numerical simulation (bottom)] of 3 µm particles in a 15 µm microchannel constriction for various pure DC voltages: (a) 200 V, (b) 400 V, (c) 600 V and (d) 800 V.

Particle motion is affected by the size of the channel and Joule heating effects. In 45 µm depth microchannel particles are dispersed further when compared to the shallow 15 µm depth microchannel. Joule heating increases when the size of the channel increases because of the high volume to surface area ratio. The low conductivity PDMS does not quickly transports the internally generated heat to the surroundings. At higher voltages joule heating induced temperature gradients are higher near the constriction and it propagates the electrothermal force. Electrothermal force is always directed away from the constriction and there by suppressing the negative dielectrophoretic effect which

in turn affects the particle motion. In the fig. 3-2 (a-d), it can be clearly seen that the particle stream width is wider after exiting the constriction even at a voltage of 800 V DC. Electrothermal force at the downstream constriction end suppresses the negative DEP effect and thereby affecting the particle motion. The joule heating effect on the particle motion can be clearly seen in DC biased AC electric fields.

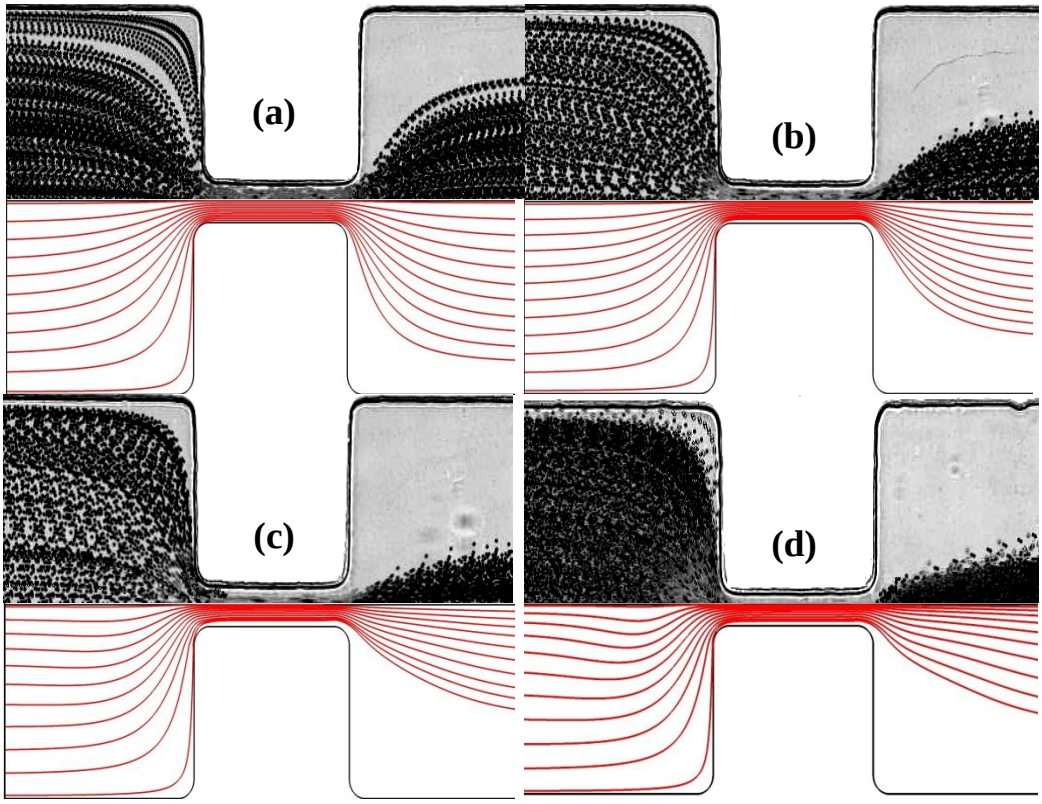

Fig 3-2: Motion (experiment (left) and numerical simulation (right)) of 3 µm diameter particles in a 45 µm microchannel constriction for various pure DC voltages: (a) 200 V, (b) 400 V, (c) 600 V and (d) 800 V.

3.5.2 Particle motion at various DC biased AC voltages

Fig. 3-4 and 3-5 compares the results of numerical simulation and experiments on motion of 3 μm diameter particles in a 15 and 45 μm depth microchannels under DC biased AC voltages. All the other parameters are fixed except the one which is to be varied. In examining the effect of the electric field ratio on particle motion, total voltage through the channel was fixed to 500 V and AC to DC voltage ratio was varied from r = 0 to 9. As expected from the negative DEP effect, particles travel in a confined stream width after exiting the constriction when r is increased. It is, however, important to note that increasing r decreases the DC field component and hence reduces the throughput. The simulation results in Figure 3-4 and 3-5 (right column) show the same trend as in the experimental images. In all cases, the simulated particle trajectories agree with the experimental results, which justify the use of the correction factor in the modeling. In the figure 3-4 (a-c), i.e., ratio r= 0 to 4, particles focuses to the center of the channel as the negative DEP pushing the particles towards the center. This is because lower the electrokinetic velocity better is the particle focusing. The particle trajectory is not affected by electrothermal effects in the shallow 15 μm depth channel. For a ratio of r=9 particles are being trapped at the upstream constriction end as negative DEP force dominates the electrokinetic velocity. Even though DC component is the driving force for the fluid, at this ratio particles are trapped because of large DEP effects.

But a different trend is observed in 45 µm depth channel shown in the figure 3-5 (a-d), i.e., ratio r= 0 to 9, particles tend to follow a single line instead of being trapped. Particle motion in larger depth channel is affected by two parameters, size and Joule hating. Electrothermal forces are high at higher AC voltages than at pure DC voltages because fluid convection takes away most of the heat in pure DC field. At this high AC voltage electrothermal force is high because of locally amplified electric field in the constriction region. In large depth channels of same applied electric field, negative DEP force will be lesser when compared to shallow depth channel. Therefore particles are not rapped even ta low DC magnitudes. They follow a streamline path affected by electrothermal force. Along the constriction ends particles gets deflected and makes the stream width wider. Increasing the AC field results in the increase of Joule heating which may cause potential harm to the live cells which are being tested.

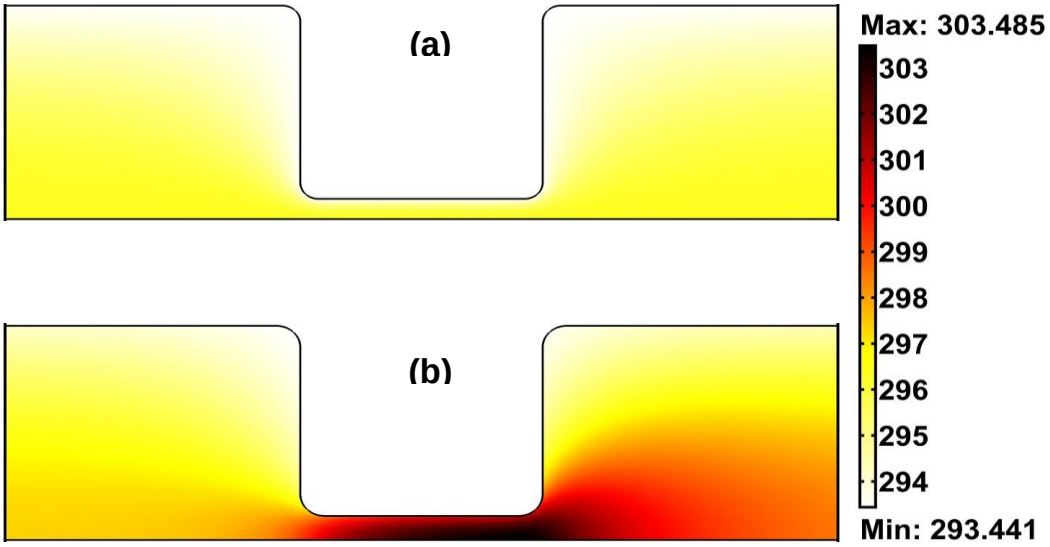

Fig. 3-3: Contour plot of temperature distribution in 15 µm (a) and 45 µm (b) depth microchannel constrictions.

To emphasize the effect of Joule heating a temperature contour plot is presented for 15 and 45 µm depth channels for DC voltage of 500 V in the fig. 3-3. The temperature rise difference between the two channels is around 7 K. The temperature in the 45 µm is not symmetric about constriction because of the convection term included in the eq. 12. The maximum temperature region shifts towards the downstream end depending upon the electric field magnitude.

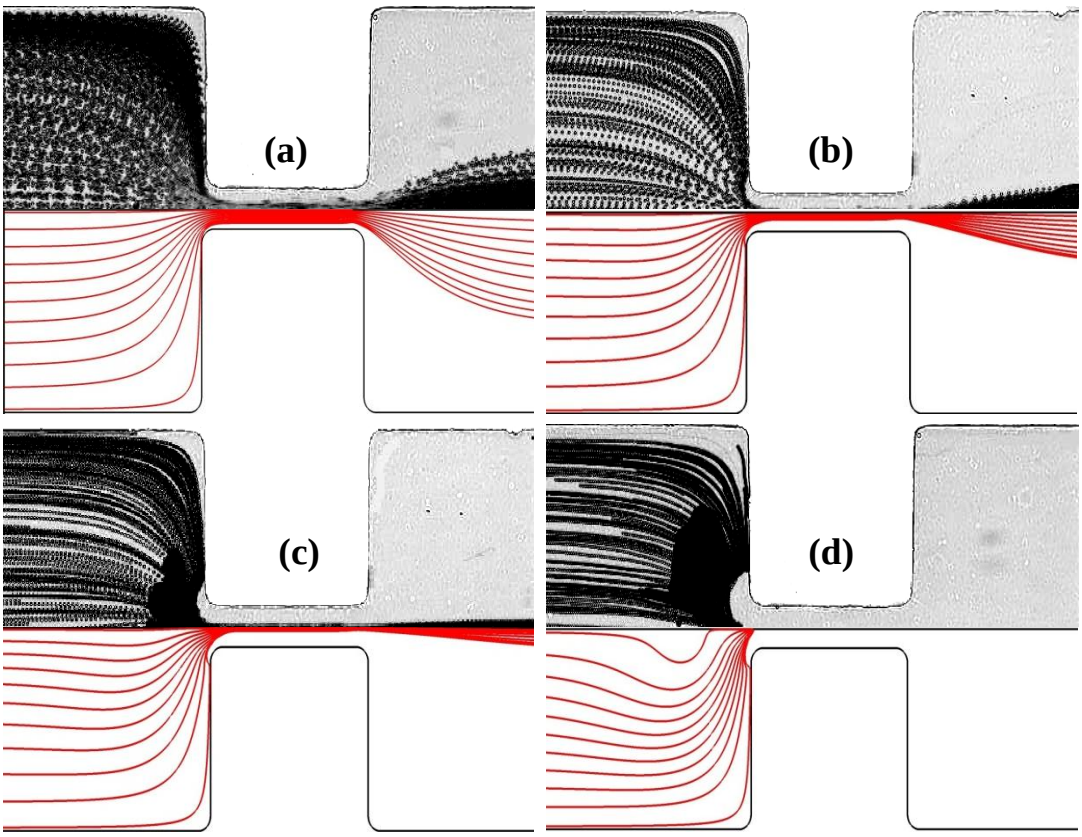

Fig. 3-4: Motion (experiment (left) and numerical simulation (right)) of 3 µm particles in a 15 µm depth microchannel constriction for various DC biased AC voltages: (a) 500 V DC (r=0), (b) 166 V DC/334 V AC (r=2), (c) 100 V DC/400 V AC (r=4), and (d) 50 V DC/450 V AC (r=9).

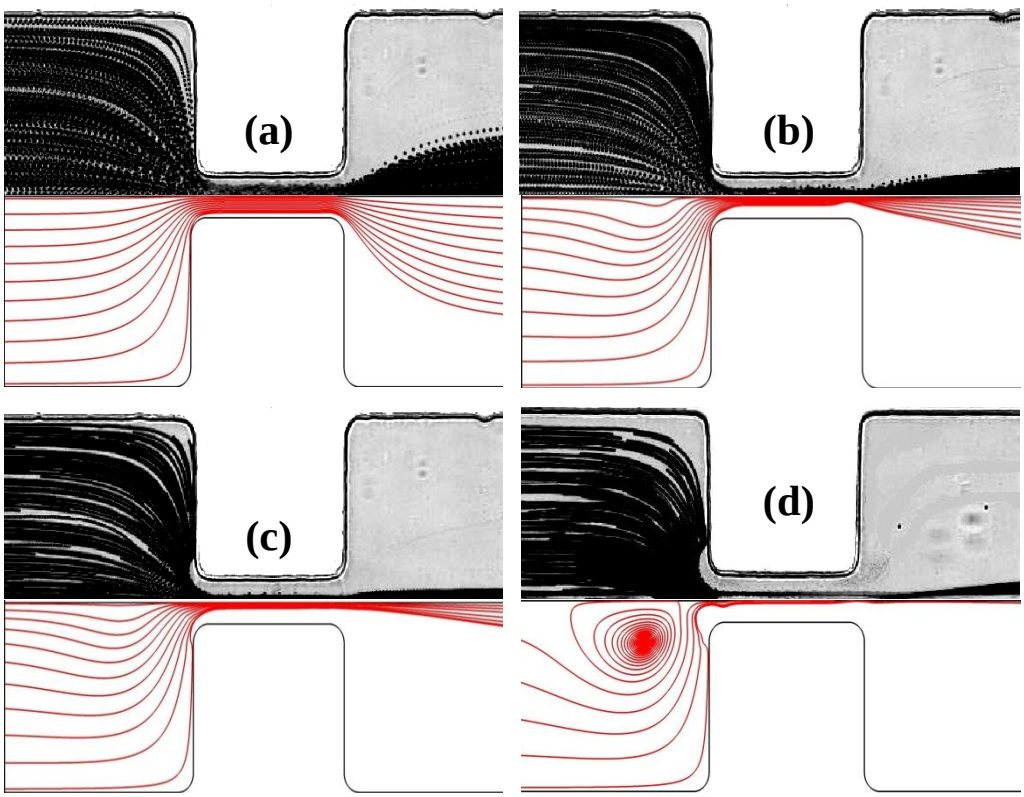

Fig. 3-4: Motion (experiment (left) and numerical simulation (right)) of 3 µm particles in a 45 µm depth microchannel constriction for various DC biased AC voltages: (a) 500 V DC (r=0), (b) 166 V DC/334 V AC (r=2), (c) 100 V DC/400 V AC (r=4), and (d) 50 V DC/450 V AC (r=9).

3.6 Summary

A comparative study has been performed by numerical simulation and experiments on motion of 3 µm particles in a 15 and 45 µm depth microchannels for various DC and DC biased AC voltages. It has been observed that the particles in 15micron depth channel does not experience joule heating and tend to follow a confined path after exiting the constriction. Negative DEP dominates the electrokinetic motion of particles which traps the particles at lower DC magnitude. While the particles in 45 micron depth dispersed after exiting the constriction due to joule heating effects. Electrothermal effects take its toll in 45

micron depth channels due to the large volume to surface area ratio. Even at higher AC voltages particles follow a single stream line path coming out form the constriction. This greatly affects the live cells which are being experimented. In order to avoid the joule heating effect researchers tend to use very dilute solutions.

CHAPTER 4

JOULE HEATING EFFECTS ON ELECTROKINETIC SAMPLE MIXING IN CONSTRICTION MICROCHANNELS

4.1 Introduction

Microfluidics is the study of fluid flow in geometries of dimensions in the order of micro and nanometers. Electrokinetic methods in LOCs are used for operation like pumping, separation, filtering and sorting. One of the high challenges in microfluidics is the mixing of two fluid streams. Generally, electrokinetic flows are laminar because of their reduced geometry and low Reynolds number. Mixing in such a laminar flow can occur only through diffusion and it has raised a challenging need to produce an effective mixing at micro level

Rapid mixing is essential in many lab-on-a-chip devices used in, for example, biochemical assays and chemical reactions etc. However, due to the low Reynolds number flow typically encountered in microfluidics, mixing of samples in different fluid streams often takes place through molecular diffusion only. The time scale for such diffusive mixing is determined by L^2/D, where L is the diffusion length and D is the diffusion coefficient of the sample molecules. Therefore, a sample with a typical $D = 1\times10^{-10}$ m^2/s will need 400 s to diffuse across the half width of the microchannel (i.e., 200 μm) we used in the preliminary experiment. Certainly, decreasing the channel width will dramatically reduce the mixing time (e.g., the diffusion time across the half width of the 40 μm

wide constriction drops to 4 s), which, however, greatly increases the flow resistance and lowers the throughput. Therefore, numerous approaches have been developed for microfluidic mixing and can be classified as passive or active [73, 74]. In passive mixing there is no external energy required. It can be achieved through diffusion or convection. In active mixing, external source such as micro pumps, ultra sound and acoustic vibrations are being used. Passive mixers utilize complex channel geometries to promote mixing, which subject the fluid streams either to repeated splitting and recombination [75, 76] or to chaotic advections in staggered or curved microchannels [77-80]. Active mixers rely on an external force, such as acoustic [81], magnetic [82], electrokinetic [83] forces, to switch on and off the mixing. The fluid streams are usually actuated by one or more syringe pumps. Droplets have also been demonstrated to implement a rapid mixing using winding microchannels [84] or electrowetting [85].

In the recent past, mixing has been achieved through various techniques. Wu and Li [86] demonstrated the micro mixing using induced charge electrokinetic flow. The results show that circulations generated from the induced non-uniform zeta potential distribution along the conducting hurdle surfaces provided efficient mixing between different solutions. The degree of mixing enhancement depends upon the hurdle geometries and hurdle numbers. Jeon and shin [87] presented a design and simulation of passive mixing in microfluidic systems with geometric variations. Recently Naher [88] demonstrated micro scale mixing in three different geometries. The results showed the degree of

mixing depend on channel geometry when parameters such as inlet velocity, viscosity and pressure were kept constant. In geometries with hurdles provided lateral pressure and swirling vortices which provided better mixing results.

Mixing can also be achieved through electrothermal effects. Suspending medium in the channels is affected by Joule heating due to the locally amplified electric field around micro electrodes or in-channel structures. Joule heating can elevate the buffer temperature and disturb the electroosmotic flow causing significant sample dispersion. A pair of counter-rotating fluid circulations could form near the microelectrodes or in the regions of high temperature gradients [39] called electrothermal flow generated due to the Joule heating-induced gradients of fluid conductivity and permittivity under AC electric fields [40,41]. Its magnitude is proportional to the fourth power of the local electric field. They have been recently demonstrated to enhance microfluidic mixing [44] and immunoassays [45] and to pump bio fluids [46,47] as well.

4.2 Theory

The governing equations for the coupled electric, heat and fluid flow which are responsible for the electrokinetic transport phenomena have been previously explained in the theory section of chapter 2. The following paragraph presents the governing equation for the convection and diffusion which is responsible for the sample mixing.

4.2.1 Convection Diffusion equation

The steady state convection diffusion equation is given as [3]

$$\left(\mathbf{u}+\mathbf{u}_{ep}\right)\nabla \mathrm{c}=\nabla\bullet\left(\mathrm{D}\nabla \mathrm{c}\right) \tag{21}$$

Where, c is the concentration, u is the velocity field, u_{ep} is the electrophoretic velocity of the sample and D is the diffusion coefficient of the sample. The convection term in the above equation is many times higher in magnitude than that of the diffusion term. So the velocity field should give a good indication of concentration distribution in the channel. The governing equations of coupled electric, temperature, flow field and concentration fields were solved using COMSOL multiphysics finite element software. Rhodamine B dye has a diffusion coefficient of 4.5e-10 m^2/s which is being used to estimate the concentration fields in 5 mM buffer solution. The chosen sample is considered neutral and is not affected by application of electric field, so the electrophoretic velocity term in the above equation is dropped.

Mixing efficiency is calculated using the formula [86]

$$\xi=\left(1-\frac{\int_0^w \left|c-c_\infty\right|dy}{\int_0^w \left|c_0-c_\infty\right|dy}\right)\times 100\% \tag{22}$$

Where c_∞ corresponds to the perfect mixing, c_0 is the concentration distribution at the inlet, c is the concentration distribution at some distance downstream from the constriction.

4.3 Numerical model and Boundary conditions

To understand the phenomenon of the electrokinetic sample transport and mixing of fluids a numerical model was developed. COMSOL 3.5a multiphysics software was used to carry out the simulation. It is a comprehensive tool for solving problems involving multiphysics and used especially in the field of microfluidics. Since type of flow is laminar in microfluidic transport, COMSOL provides reasonable solution for steady and unsteady flows. Conductive media DC, convection diffusion, incompressible Navier-Stokes and convection diffusion equations modes were selected to solve for the EK transport and mixing of fluids. A 2D geometry was created using the drawing tools and the dimensions of which are explained previously. As shown in fig. 4-1 the geometry consists of two inlets 200 µm wide which extends for 1 mm and join into single channel at the T junction. From the T junction the length of the channel is 1 mm and 400 µm wide at the center cross section area is reduced to form a constriction. One of the inlets is supplied with Rhodamine B dye with a concentration of 1 mol/m^3 which has a diffusion coefficient of 4.5e-10 m^2/s. Two microchannels, one with 15 µm depth and other with 45 µm are under consideration. 3D geometries leads to complexity in modeling and take more computational time, a simplified 2D geometry was created as mentioned earlier. This model is sufficient enough to capture the main feature of EK sample transport and mixing. The geometry was then meshed with triangular meshes using the free mesh parameters tool box. The domain is finely meshed with 240,000 elements with the maximum element

size of 5e-6 m. Model validation was done by increasing the number of mesh elements ranging from 5,000 to 350,000. As noted earlier, only the fluid phase in the numerical model is considered and solved for the coupled electric, temperature, flow field and diffusion equation in two-dimension for simplicity.

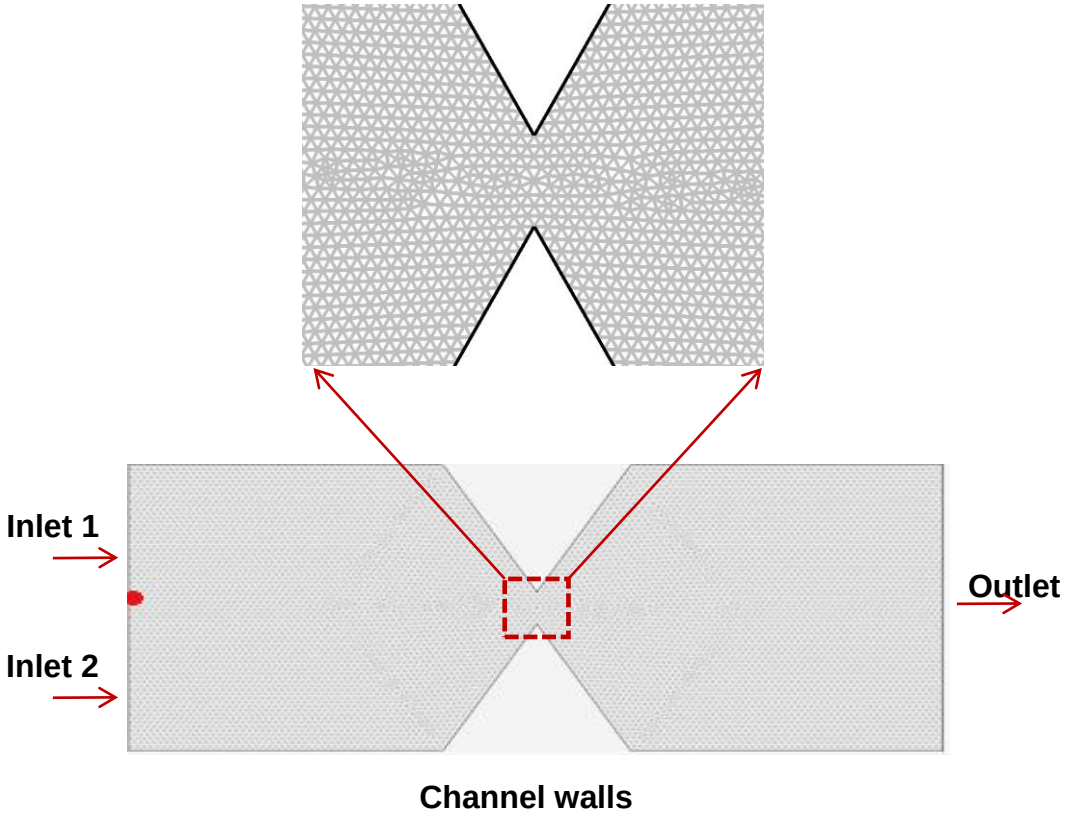

Fig. 4-1: Meshed microchannel geometry with inset showing the zoom in view of the quality of mesh.

4.3.1 Conductive media DC

Inlet 1 and 2: $\phi = V_0$, and outlet: $\phi = 0$. Where V_0 is the applied electric potential and outlet is grounded.

Channel wall: $\mathbf{n}\bullet(\sigma\nabla\phi) = 0$, is electrically insulated, where **n** denotes the unit normal vector.

4.3.2 Convection and Conduction

Inlet 1, inlet 2 and outlet: $T = T_0$, i.e., the fluids in the end-channel reservoirs are assumed isothermal as their volumes are much larger than the fluid within the microchannel [49,53].

Channel wall: $q'' = -h(T - T_0)$, where q'' is the outward heat flux due to heat convection with an assumed heat transfer coefficient h. The magnitude of h is determined by matching the model predicted rise in electric current with the experimentally measured data. This value is assumed constant throughout the channel wall and independent of the fluid temperature for simplicity.

4.3.3 Incompressible Navier-Stokes

Inlet 1, inlet 2 and outlet: $\mathbf{n}\bullet(\eta\nabla\mathbf{u}) = 0$ and $p = 0$, i.e., the fluids in the end-channel reservoirs are assumed to have zero viscous stress and zero pressure.

Channel wall: $\mathbf{u} = \varepsilon\zeta\nabla\phi_{DC}/\eta$, where ζ is the zeta potential of the channel wall. This is a slip boundary condition for electroosmotic flow in microchannels with thin electric double. Both the DC and AC components generate Joule heating and contribute to electrothermal flow via the electrothermal force. This indicates that the strength of electrothermal flow can be varied by adjusting the DC to AC field ratio, which will be demonstrated in the results section.

4.3.4 Convection and Diffusion

Inlet 1, c = c0 and inlet 2, c= 0, Where c0 is the applied concentration in mol/$m^{3.}$ Channel walls are applied with insulation boundary condition and outlet is applied wit convective flux which means the outlet concentration is unknown.

4.3.5 Temperature dependent properties

Temperature dependent properties which are responsible for the joule heating and the electrokinetic transport have been discussed in the earlier chapters. The table shown below displays the constants used in the numerical simulation. The convective heat transfer coefficient was determined the same way as it was done for the previous chapters.

Name	Value	Unit	Description
D	4.5e-10	m^2/s	Diffusion coefficient
h1	20e3	W/m^2K	Convective heat transfer coefficient
h2	2000e3	W/m^2K	Convective heat transfer coefficient
σ_0	0.05	S/m	Fluid electric conductivity at T_0

Table 4.1: Shows the list of constants used in the numerical simulation of Joule heating effects on electrokinetic sample mixing.

The convective heat transfer coefficient was determined the same way as discussed in the chapter 2

4.4 Results and discussion

This section presents the parametric study effects of electric field, channel depth and constriction shape on sample transport and mixing in constriction microchannel. The electric field effects examined include DC magnitude and DC

biased AC voltages. All the parameters are fixed except the one which is to be varied. Mixing efficiency is also calculated for each case to determine the effective mixing.

Fig. 4-2 shows the contour plot of concentration distribution comparing a 45 μm depth triangle shaped constriction microchannel with and without joule heating effect and 45 μm depth straight microchannel for a voltage ratio of 100 V DC and 400 V AC . The three datum plots are shown to emphasize the effectiveness of sample transport and mixing with inclusion of electrothermal body force due to joule heating. It can be seen from the figure that triangle shape constriction channel with Joule heating effects shows a better mixing because of the formation of vortices at constriction ends. This is because of amplified electric field in the constrained region to compensate the conservation of current equation and the Joule heating induced temperature gradients. Diffusion is a slow process in the microfluidics because of low Reynolds number and reduced geometric length scale. So a straight channel takes a longer time and requires a long channel to enhance effective diffusion and mixing. Figure 4-3 shows the concentration profile at a downstream distance of 6.5 mm from the entrance of the channel. The 45 μm depth channels shows greatest degree of mixing with efficiency of 80.5 % for a ratio 100 V DC and 400 V AC while the straight channel and triangle shape channel without Joule heating hardly showed signs of mixing or diffusion. The efficiency was found to be 28.3 % and 32.4 % respectively.

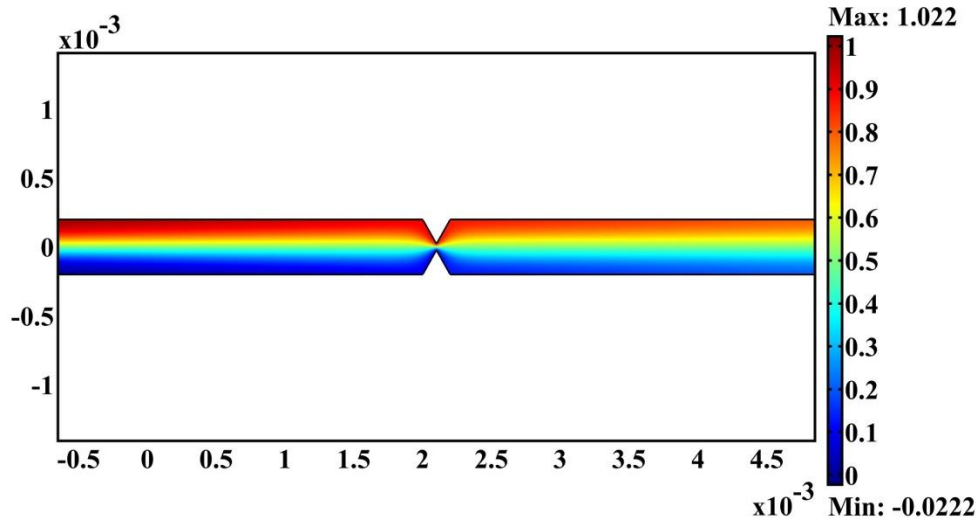
x10^-3
1
0.5
0
-0.5
-1
-0.5 0 0.5 1 1.5 2 2.5 3 3.5 4 4.5
x10^-3
Max: 1.022
1
0.9
0.8
0.7
0.6
0.5
0.4
0.3
0.2
0.1
0
Min: -0.0222

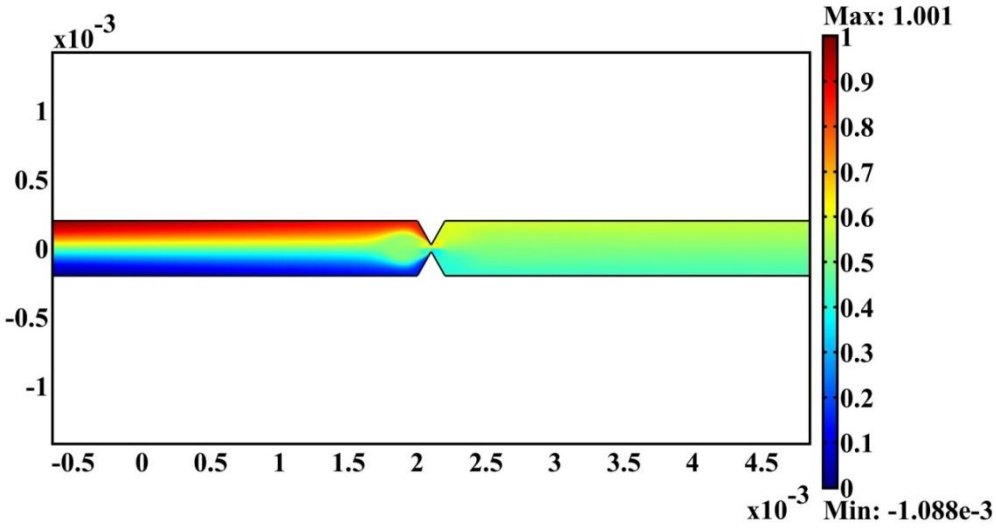
x10^-3
1
0.5
0
-0.5
-1
-0.5 0 0.5 1 1.5 2 2.5 3 3.5 4 4.5
x10^-3
Max: 1.001
1
0.9
0.8
0.7
0.6
0.5
0.4
0.3
0.2
0.1
0
Min: -1.088e-3

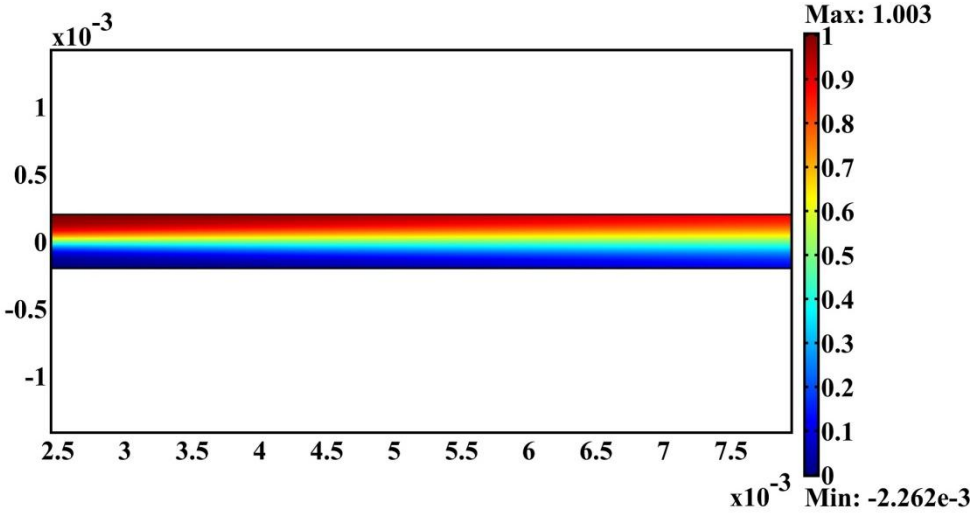
x10^-3
1
0.5
0
-0.5
-1
2.5 3 3.5 4 4.5 5 5.5 6 6.5 7 7.5
x10^-3
Max: 1.003
1
0.9
0.8
0.7
0.6
0.5
0.4
0.3
0.2
0.1
0
Min: -2.262e-3

Fig. 4-2: Concentration fields for triangle shaped constriction without (top) and with (middle) Joule heating and straight channel (bottom) under a voltage ratio of 100 V DC and 400 V AC for a 45 µm depth. The legend indicates the concentration field across the entire channel.

These datum case has been used a base for the parametric study of Joule heating effects on mixing. To evaluate numerical model experiments are being conducted in our lab currently with different channel shapes, structures and electric field. From this simulation it has been observed that even channel structure contributes the mixing which will be dealt later in the following paragraphs.

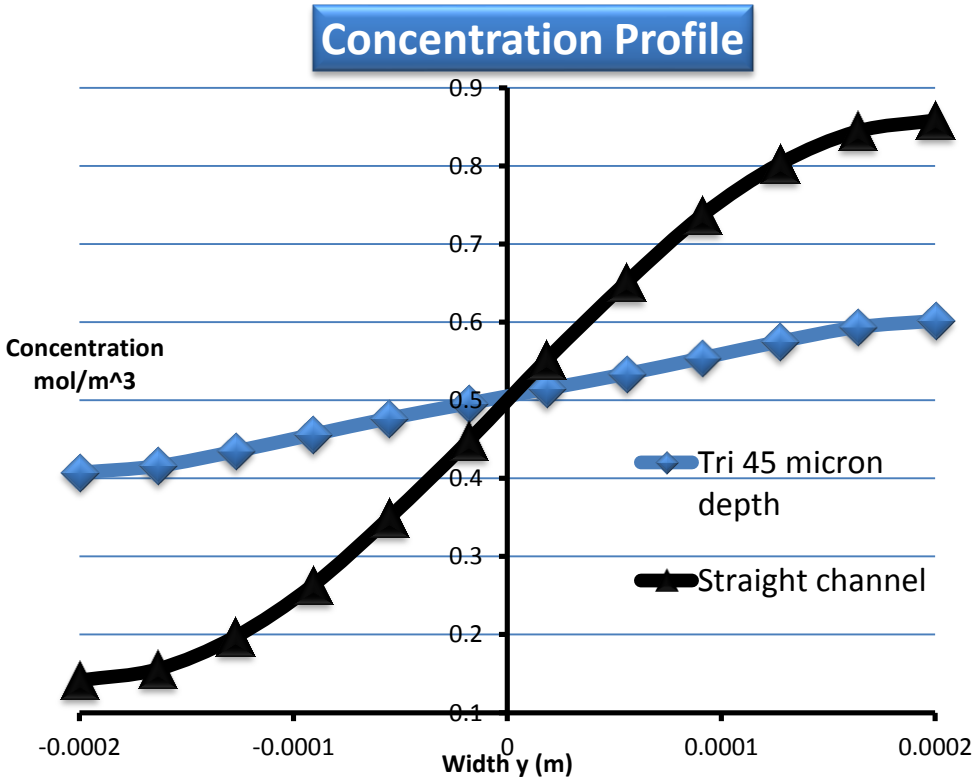

Fig. 4-3: Concentration profile across the channel width at a downstream position of 6.5 mm from the channel entrance under an applied voltage ratio of 100 V DC and 400 V AC for triangle shaped constriction channel and straight channel of 45 µm depth

4.4.1 Effect of channel depth

Fig. 4-4 shows the concentration profile across the channel width at a fixed downstream position of 1 mm from the constriction for a voltage ratio of 100 V DC and 400 V AC . Figure shows the case for single constriction comparing 15 μm and 45 μm depth microchannels. As expected the 45 μm depth channel gives the greatest degree of mixing with a mixing efficiency of 80.5 % and the 15 μm depth channel gives 62.3% efficiency. Mixing is enhanced by two parameters one being the structure of the channel and other being the Joule heating effect. Even though there is no Joule heating in 15 μm depth channels there is a 62.3 % mixing efficiency due to the structure of the channel. Larger the channel depth more the generation of Joule heat leading to better mixing due to the formation of vortices at the ends of constriction. Joule heating is higher in larger depth channels because of high volume to surface area ratio. The internal generated heat cannot be dissipated at a faster rate. This is illustrated with the contour plot of temperature and streamline plot of velocity field in the figure 4-5. As it can be seen from the fig. 4-5 (top) that maximum temperature occurs in the center of the constriction where the electric field is locally amplified and gradually reaches room temperature away from the constriction. Streamline plot of velocity field (fig. 4-5 (bottom)) gives better understanding of mixing because it is several orders of magnitude larger than the diffusion term. Vortices are formed on both ends of the constriction due to the joule heating induced temperature gradients which greatly

enables mixing. This type of flow cannot be observed in shallow 15 µm depth channel as the flow is not affected by temperature gradients.

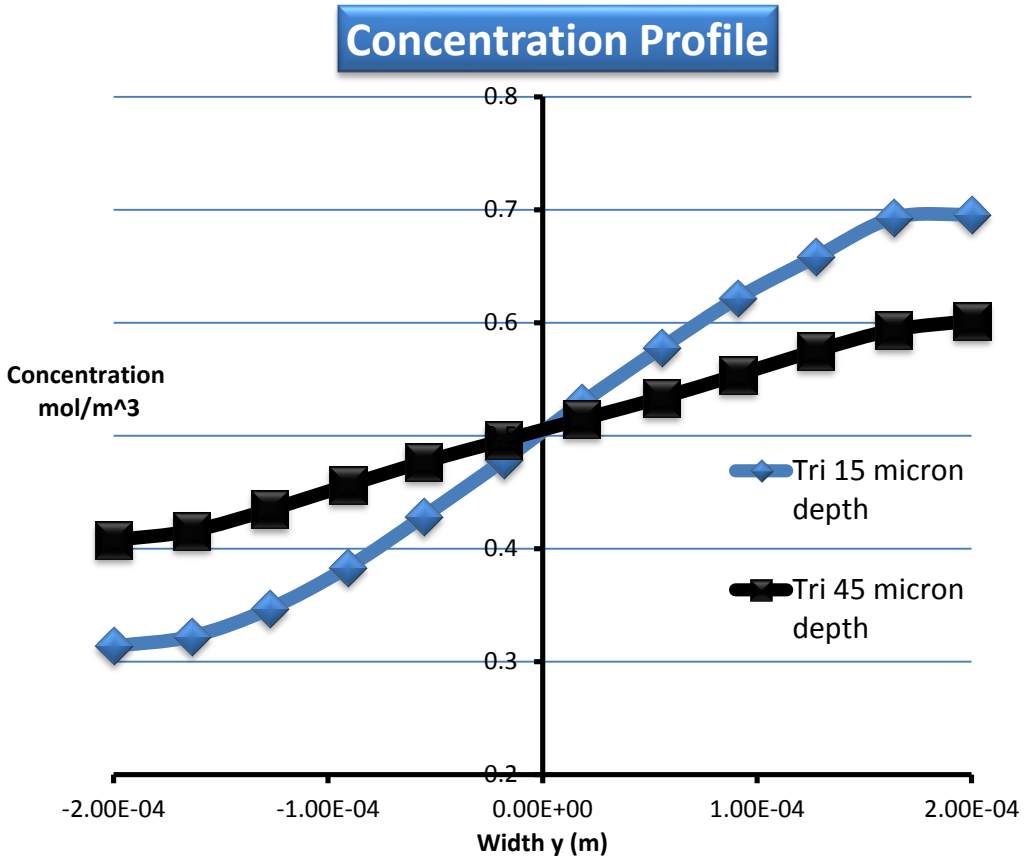

Fig 4-4: Concentration profile across the channel width at a downstream position of 1mm from the constriction under an applied ratio of 100 V DC and 400 V AC for 15 and 45 µm channel depth.

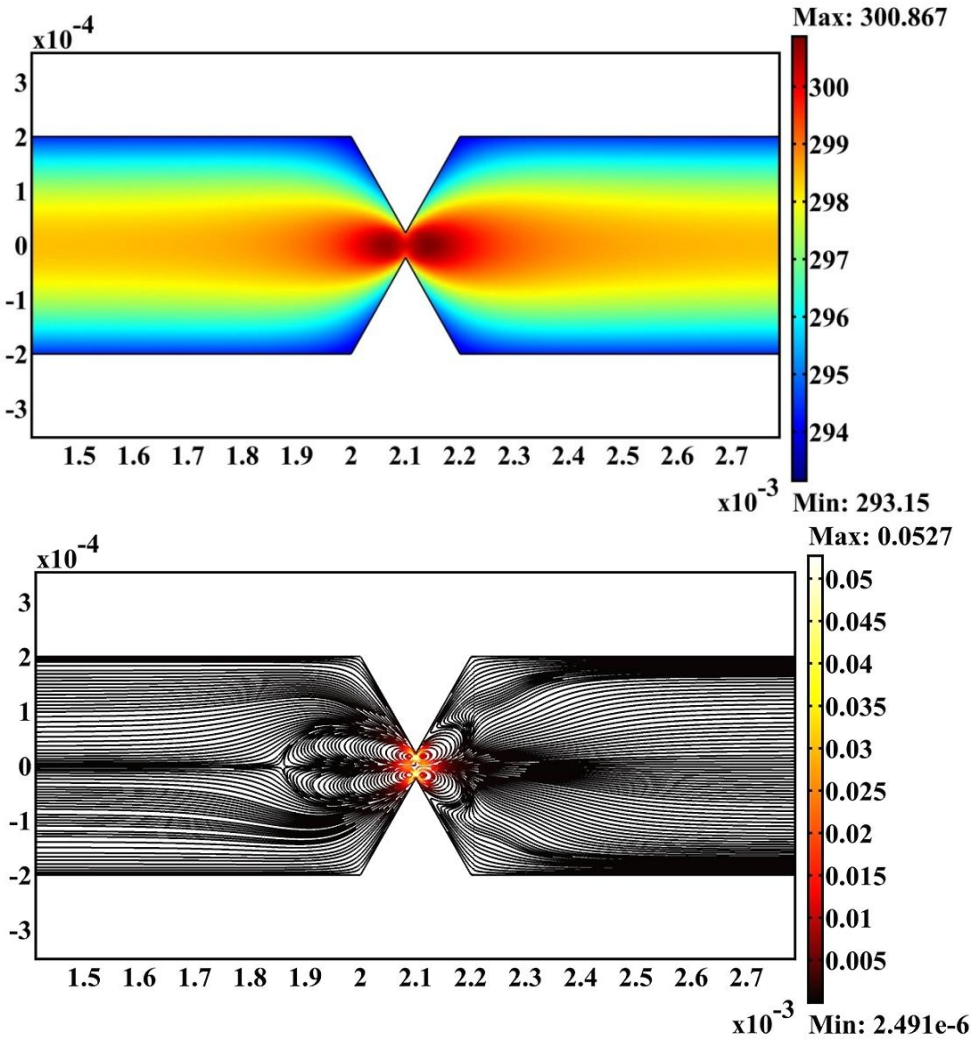

Fig. 4-5: Shows the contour plot of temperature (top) and the streamline plot of velocity field (bottom) for a triangular shaped constriction channel of 45 µm depths the legends on both the figure indicating the magnitude temperature distribution and velocity field in the channel respectively.

4.4.2 Effect of channel structure

A study of channel shape effects on the mixing is also presented. Fig. 4-6 shows the contour plot of 45 micron depth rectangle shaped constriction. And for the triangle shaped one is shown in the fig. 4-2. From the channel shape

comparison it was determined that triangle shapes constriction channel of 45 µm depth showed better mixing, i.e., almost 20 % higher mixing than its counterpart. From the streamline plot in fig. 4-5 multiple vortices are formed at both the ends of the constriction region when compared to rectangle shaped constriction which forms only two vortices at the downstream of the constriction.

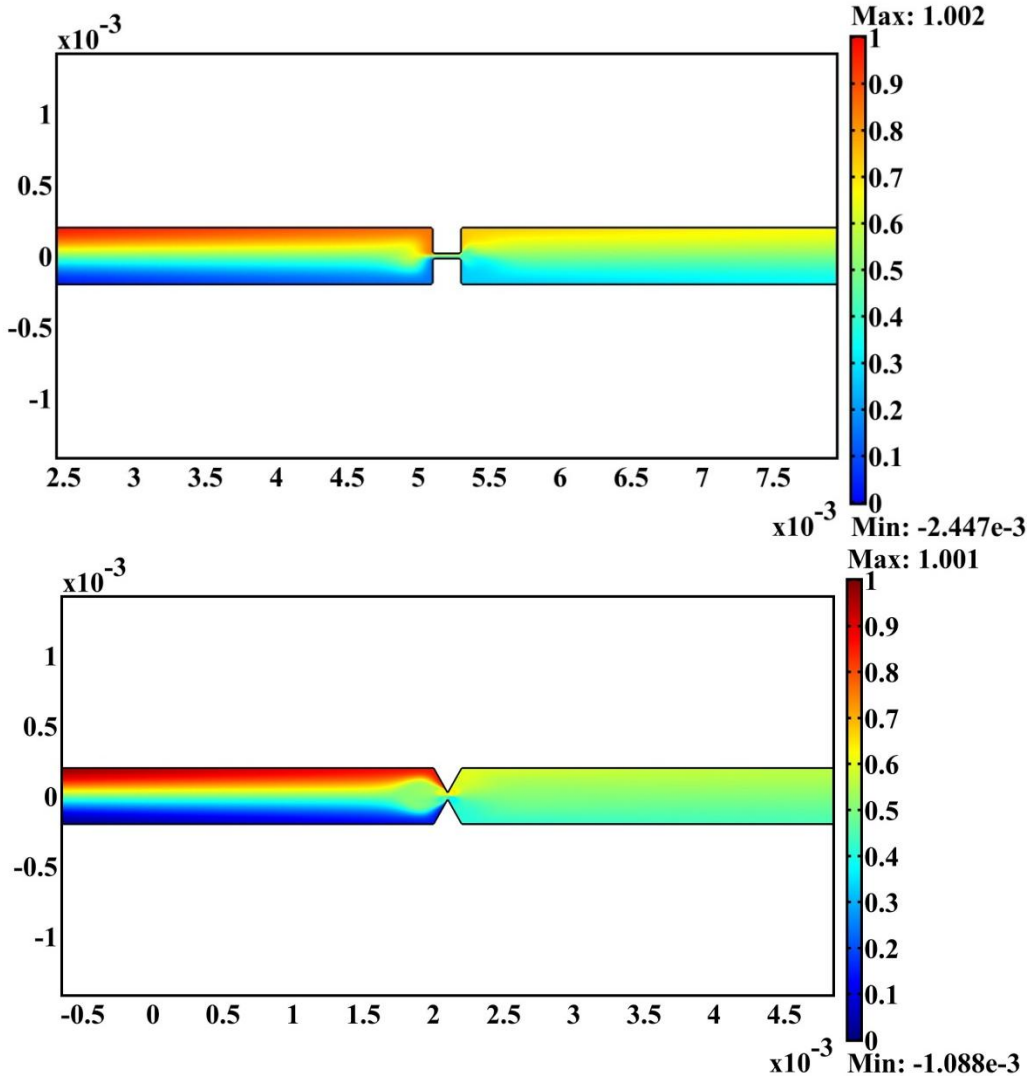

Fig. 4-6: Concentration field for rectangle and triangle shaped constriction microchannels of 45 µm depth. The legends indicate the concentration field across the channel.

4.4.3 Effect of constriction numbers

If the single constriction is replaced by a series of constrictions placed at regular intervals, the species mixing can be further enhanced. Fig. 4-8 shows the concentration profile across the channel width at the downstream position of 1mm with two constrictions and a gap of 1mm between them. The mixing efficiency of the triangular constriction increased to 99 % and that of rectangular constriction increased to 70.2 % respectively which are much higher than the single constriction channels which produced 80.5 % and 59.3 % respectively. The use of double constriction produces multiple vortices at every constriction ends which is already two times the one produced using single constrictions. This will obviously increase the mixing efficiency by enhancing faster diffusion. This is shown as a streamline plot of velocity field in a double triangular shaped constriction channel in the fig. 4-7.

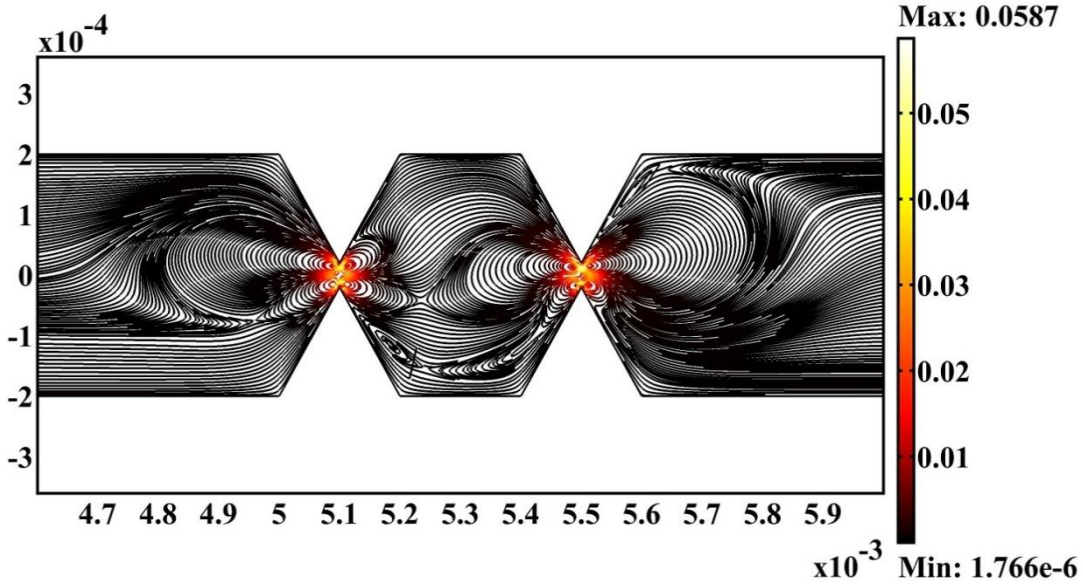

Fig 4-7: Streamline plot of velocity field for a double triangular shaped constriction channel of 45 µm depth under a voltage ratio of 100 V DC and 400 V AC. The legends indicate the magnitude of the velocity field.

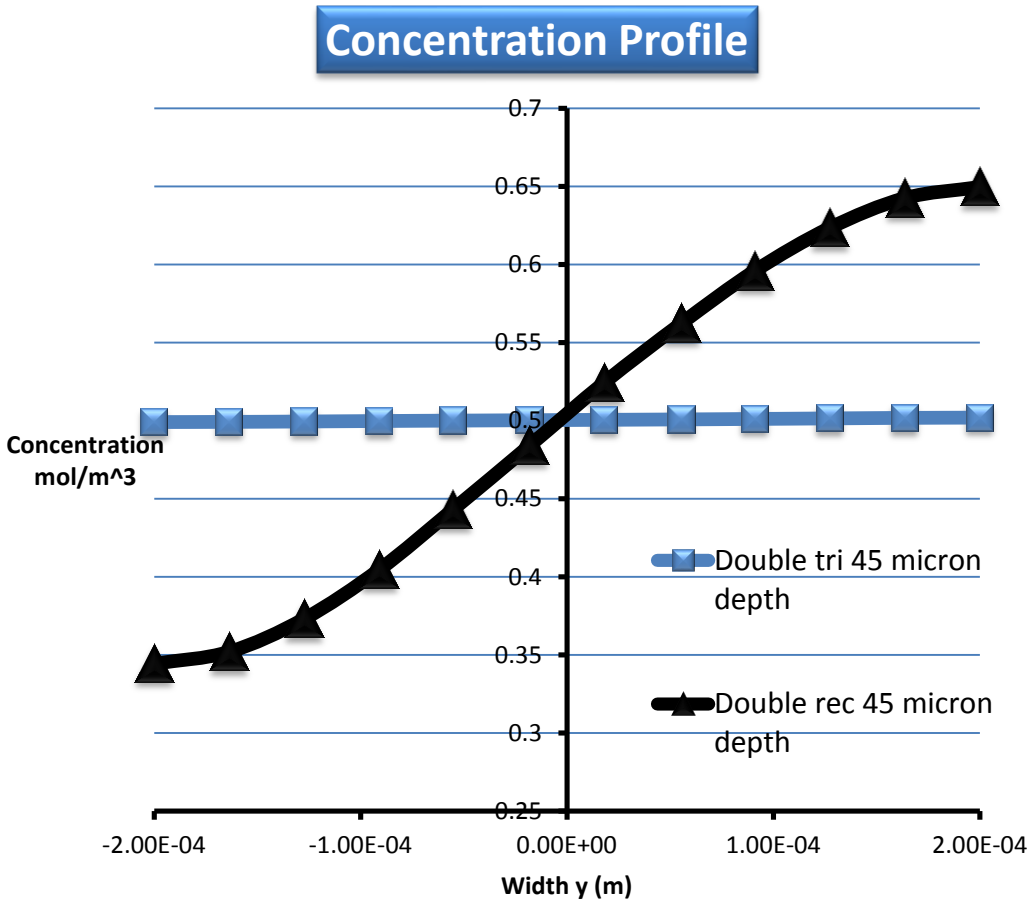

Fig 4-8: Concentration profile across the channel width at a downstream position of 1mm from the constriction under an applied voltage ratio of 100 V DC and 400 V AC for 15 and 45 µm channel depth.

4.4.4 Effect of electric field

The dependence of the mixing on the applied electric field strength was also examined. Fig. 4-9 presents the mixing efficiency for various DC voltages. As shown in the figure, under a low applied electric field triangular constriction

microchannel of 45 µm depth give high mixing efficiencies. This is because the molecular diffusion is the dominant mixing mechanism as low speed flow. For a microchannel length of 22 mm, the species can always be well mixed after a certain distance in the channel. However, if the applied electric field is increased, the fluid convection dominates the diffusion and mixing efficiency decreases rapidly since there is no circulation in the channel. Electrothermal effect can only be observed under DC biased AC voltages. The mixing efficiency starts to reduce from 64 % at 50 V DC to almost 4 % at 500 V DC.

Fig. 4-10 shows the mixing efficiency for the same microchannel under DC biased AC voltages. Decreasing the DC voltage increases the mixing efficiency because molecular diffusion takes place rapidly at low electric fields. Also the electrothermal force is seen more prominently at higher AC voltages. The more the applied AC voltage the larger the circulation formed in the constriction leading to a higher mixing efficiency. The figure shows the efficiencies for cases ranging from 25 V DC and 475 V AC to 100 V DC and 400 V AC. The plot shows 99 % efficiency for 25 V DC and 475 V AC case and gradually reduces for increasing DC magnitude.

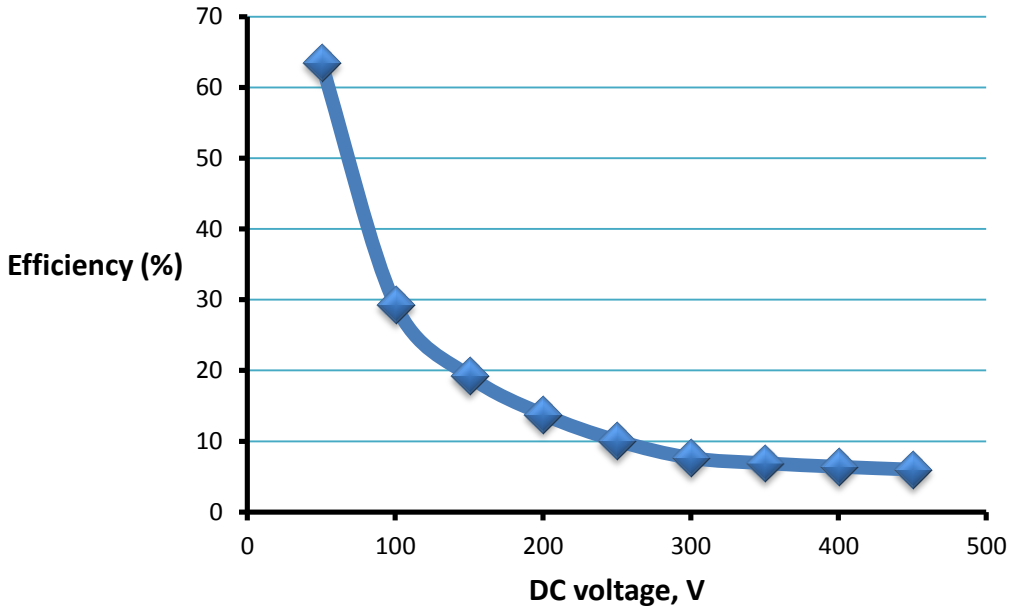

Fig. 4-9: Dependence of mixing efficiency on applied DC electric field for triangular shaped constriction microchannel of depth 45 µm

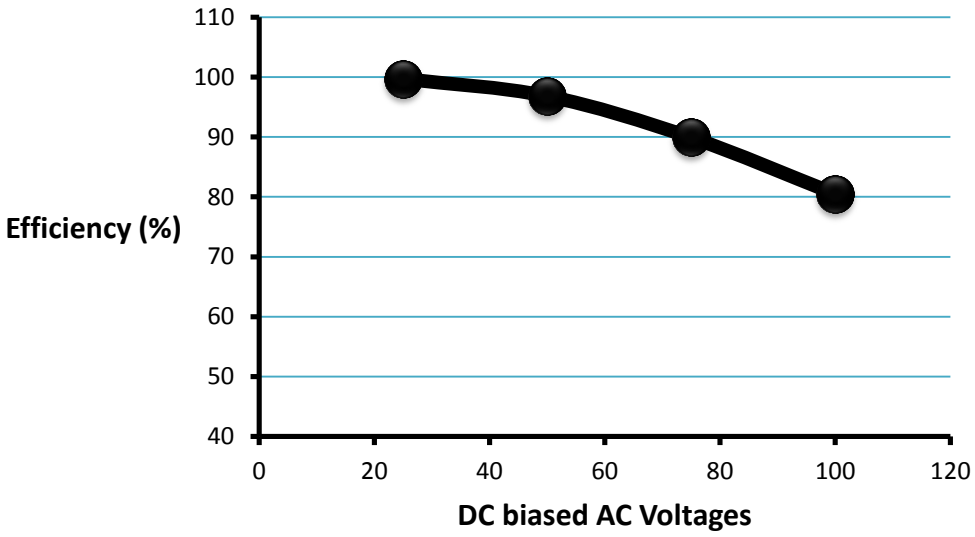

Fig 4-10: Dependence of mixing efficiency on applied DC biased AC electric field for triangular shaped constriction microchannel of depth 45 µm

4.5 Summary

In this work, the effective mixing performance of triangular shaped constriction microchannel was investigated through numerical simulation. A parametric study on channel depth, channel structure and electric field magnitude was conducted to estimate the effective mixing of samples. The numerical results show that the triangle shaped constriction microchannel with a depth of 45 μm gave better mixing with the assistance of Joule heating induced electrothermal circulations near the constrictions. The effect of channel structure, channel depth and the applied field on the sample mixing was investigated numerically and it is found that degree of mixing depends on the channel structure and the magnitude of Joule heating. Joule heating is more in larger depth channels and induces high temperature gradients which are responsible for the vortices at low DC and high AC voltages. Also, the mixing can be further enhanced by introducing multiple constrictions in series because it produces more flow vortices near the constrictions.

CHAPTER 5

CONCLUSIONS AND FUTURE WORK

This thesis presented a combined experimental and numerical study of Joule heating effects on electroosmotic fluid flow, particle electrokinetic transport and sample mixing in constriction microchannels. The main conclusion of this work is to extend the scope of microfluidics approach in manipulating cells and particles by electrokinetic means. This thesis mainly concentrates on the interaction between fluids and the electric field coupled with Joule heating and electrothermal force in constriction microchannels. In iDEP, both DC and AC voltages can be applied to the remote electrodes positioned in end-channel reservoirs for transporting and manipulating particles. The electric field gradients are caused by the blockage of electric current due to in-channel hurdles, posts, and ridges. However, iDEP devices suffer from the issue of Joule heating due to locally amplified electric field around the microelectrodes or insulators.

The second chapter presented a parametric study of Joule heating effects on the electroosmotic flow in insulator based dielectrophoresis under AC and DC biased AC voltages. It was determined that increasing the AC voltages results in increase of Joule heating induced temperature gradients of conductivity and permittivity. These temperature gradients in turn generate electrothermal body force which results in swirling motion of fluid on both ends of constriction. Therefore low conductivity solutions or low concentration solutions are

recommended for researchers in order to avoid the effect of Joule heating. Similarly by reducing the DC component in DC biased AC voltages results in electrothermal and electroosmotic flow along the ends of the constrictions. This type of flow can be of useful in sample transport, immunoassays and mixing of two fluid streams. Moreover a study was also conducted on the joule heating effects of size of the constriction. It was determined that increasing the width of the constriction resulted in less Joule heating which suitable for conducting experiments with live biological cells.

The third chapter discussed a parametric study of Joule heating effects on negative dielectrophoresis and electrokinetic transport in two different constriction microchannels. In this work we examined particle trajectories as a result of electroosmotic, electrophoretic and dielectrophoretic phenomena with coupled Joule heating and electrothermal flow effects in iDEP devices of 15 and 45 μm depths. The use of channel size has been examined experimentally and numerically. Results indicate that electrothermal effects can alter the particle trajectories depending upon the electric field applied. From this work it was proven that larger depth channels possess higher Joule heating because of high volume to surface area ratio and inability of the PDMS substrate to transport heat to the surroundings. Particle trapping is a strong function of channel size and it is affected by electrothermal flow. This work suggests the use of smaller channel depth for particle trapping and larger channel depth for controlled focusing of particles exiting the constriction at a high AC to DC Voltage ratio.

The fourth chapter presented a numerical study of joule heating effects on the electrokinetic sample mixing. In this work, effective mixing performance of two fluid streams was investigated by numerical simulation for various channel geometries. Results indicate that mixing is a function of channel size, structure, diffusion coefficient and applied electric field. The simulation was performed by taking Rhodamine B dye as the sample which is mixed in 5mM buffer solution. It was determined that results showed effective mixing for larger depth channels which involves large Joule heating. At AC-DC voltage ratios Joule heating creates electrothermal swirling motion of fluid in the regions of high temperature gradients. Fluids from two separate inlets gets mixed in this region before they enter out of the constriction. Mixing also depends on the structure of the channel. Results prove that triangular shaped constriction channel gave 25 % higher mixing than the rectangular shaped constriction channel. This method of mixing is fast, reliable and does not require longer channels for diffusion to happen in course of time. This method of analyzing the mixing performance is expected to provide valuable guidelines for researchers working with the various nano particles.

The future work of this research is to implement 3D modeling to simulate electro-thermally induced flows presented in chapters 2, 3 and 4. The advantage of 3D modeling is that real boundary conditions can be applied without any compensation and promising results can be obtained to compare with the experimentation. Another future work is to effectively use the Joule heating

phenomenon for mixing of samples by carefully choosing the samples and channel structures.

REFERENCES

[1] Li, D., *Electrokinetics in Microfluidics,* Elsevier Academic Press, Burlington, MA, 2004.

[2] Berthier, J., Silberzan, P. *Microfluidics for Biotechnology*, Artech House, norwood, MA, 2006.

[3] Morgan, H., Green, N. G., *AC Electrokinetic: Colloids and Nanoparticles*, Research Studies Press, Hertfordshire, UK (2002).

[4] Kasahara, Y., Nishijima, T., *Journal of physical society of Japan*, 2011, **80**, 023708.

[5] Lian, Meng, *Microfluidic manipulation by AC Electrothermal effect,* PhD diss., University of Tennessee, 2010

[6] Masliyah, J. H., Bhattacharjee.S, *Electrokinetic and Colloid Transport Phenomena*: Wiley-Interscience, 2006.

[7] Kirby B.J., *Micro- and Nanoscale Fluid Mechanics: Transport in Microfluidic Devices,* Cambridge University Press, 2010.

[8] Xiangchun Xuan, *Electrophoresis*, 2008, **298***,* 33–43.

[9] David Erickson, David Sinton and Dongqing Li, *Lab on a Chip*.

[10] Gonzalez A, Ramos A, Morgan H, Green, N. G., Castellanos, A. C., *J. Fluid Mech.* 2006, **564**, 415-433.

[11] Pohl, H. A., *Dielectrophoresis*: *The behavior of neutral matter in non-uniform electric fields*, Cambridge University Press, 1978.

[12] Lapizco-Encinas, B. H., Rito-Palmomares, M., *Electrophoresis* 2007, **28**, 4521-4538.

[13] Hawkins, B. G., Gleghorn, J. P., Kirby, B.J., "Dielectrophoresis for cell and particle manipulations", *Methods in bioengineering: Biomicrofabrication and biomicrofluidics*, ed. J. D. Zahn, Artech Press, pp. 133-181, 2009.

[14] Pethig, R., *Biomicrofluidics* 2010, **4**, 022811.

[15] Gascoyne, P. R. C., Vykoukal, J., *Electrophoresis* 2002, **23**, 1973-1983.

[16] Hughes, M. P., *Electrophoresis* 2002, **23**, 2569-2582.

[17] Chou, C. F., Zenhausern, F., *IEEE Eng. Med. Biology Mag.* 2003, **22,** 62-67.

[18] Cummings, E. B., *IEEE Eng. Med. Biology Mag.* 2003, **22,** 75-84.

[19] Srivastava, S. K., Gencoglu, A., Minerick, A. R., *Anal. Bioanal. Chem.*, 2010, **399**, 301-321.

[20] Choi, S., Park, J. K, *Lab Chip* 2005, **5**, 1161-1167.

[21] Kralj, J. G., Lis, M. T. W., Schmidt, M. A., Jensen, K. F., *Anal. Chem.* 2006, **78**, 5019-5025.

[22] Kim, U., Shu, C. W., Dane, K. Y., Daugherty, P. S., et al., *Proc. Natl. Acad. Sci.* 2007, **104**, 20708-20712.

[23] Vahey, M. D., Voldman, J., *Anal. Chem.* 2008, **80**, 3135-43.

[24] Han, K. H., Frazier, A. B., *Lab Chip* 2008, **8**, 1079-1086.

[25] Wang, L., Lu, J., Marchenko, S. A., Monuki, E. S., et al., *Electrophoresis* 2009, **30**, 782-791.

[26] Khoshmanesh, K., Zhang, C., Tovar-Lopez, F. J., Nahavandi, S., et al., *Electrophoresis* 2009, **30,** 3707-3717.

[27] Lewpiriyawong, N., Yang, C., Lam, Y. C., *Electrophoresis* 2010, **31**, 2622-2631.

[28] Lapizco Encinas, B. H., Simmons, B. A., Cummings, E. B., Fintschenko, Y., *Electrophoresis* 2004, **25**, 1695-1704.

[29] Barrett, L. M., Skulan, A. J., Singh, A. K., Cummings, E. B., Fiechtner, G. J., *Anal. Chem.* 2005, **77**, 6798-6804.

[30] Kang, K., Kang, Y., Xuan, X., Li, D., *Electrophoresis* 2006, **27**, 694-702.

[31] Pysher, M. D., Hayes, M. A., *Anal. Chem.* 2007, **79**, 4552-4557.

[32] Hawkins, B. G., Smith, A. E., Syed, Y. A., Kirby, B. J., *Anal. Chem.* 2007, **79**, 7291-7300.

[33] Lewpiriyawong, N., Yang, C., Lam, Y. C., *Biomicrofluidics* 2008, **2**, 034105.

[34] Ozuna-Chacón, S., Lapizco-Encinas, B. H., Rito-Palomares, M., Martínez-Chapa, S. O., Reyes-Betanzo, C., *Electrophoresis* 2008, **29**, 3115-3122.

[35] Zhu, J., Xuan, X., *Electrophoresis* 2009, **30**, 2668-2675.

[36] Zhu, J., Tzeng, T. J., Xuan, X., *Electrophoresis* 2010, **31**, 1382-1388.

[37] Baylon-Cardiel, J. L., Jesus-Perez, N. M., Chavez-Santoscoy, A. V., Lapizco-Encinas, B. H., *Lab Chip* 2010, **10**, 3235-3242.

[38] Voldman, J., *Annu. Rev. Biomed. Eng.* 2006, **8**, 425-454.

[39] Kang, Y. J., Li, D. Q., Kalams, S. A., Eid, J. E., *Biomed. Microdev.* 2008, **10**, 243-249.

[40] Gaš, B., Stedry, M., Kenndler, E., *Electrophoresis* **18**, 2123-2133 (1997).

[41] Xuan, X., *Electrophoresis* 2008, **29**, 33-43.

[42] Cetin, B., Li, D., *Electrophoresis* 2008, **29**, 994-1005.

[43] Evenhuis, C. J., Haddad, P. R., *Electrophoresis* 2009, **30**, 897-909.

[44] Muller, T., Gerardino, A., Schnelle, T. H., Shirley, S. G., Bordoni, F., De Gasperis, G., Leoni, R., Fuhr, G., *J. Phys. D* 1996, **29**, 340-349.

[45] Ramos, A., Morgan, H., Green, N. G., Castellanos, *J. Phys. D* 1998, **31**, 338-2353.

[46] Green, N. G., Ramos, A., Gonzalez, A., Castellanos, A., Morgan, H., *J. Electrost.* 2001, **53**, 71-87.

[47] Castellanos, A., Ramos, A., Gonzalez, A., Green, N. G., Morgan, H., *J. Phys. D* 2003, **36**, 2584-2597.

[47] Perch-Nielsen, I. R., Green, N. G., Wolff, A., *J. Phys. D* 2004, **37**, 2323-2330.

[48] Wang, D., Sigurdson, M. Meinhart, C. D., *Exp. Fluid.* 2005, **38**, 1-10.

[49] Gonzalez, A., Ramos, A., Morgan, H., Green, N. G., Castellanos, A., *J. Fluid Mech.* 2006, **564**, 415-433.

[50] Burg, B. R., Bianco, V., Schneider, J., Poulikakos, D., *J. Appl. Phys.* 2010, **107**, 124308.

[51] Lee, H., Yun, S., Ko, S. H., Kang, K. H., *Biomicrofluidics* 2009, **3**, 044113.

[52] Garcia-Sanchez, P., Ramos, A., Mugele, F., *Phys. Rev. E* 2010, **81**, 015303.

[53] Ng, W. Y., Goh, S., Lam, Y. C., Yang, C., Rodriguez, I.*, Lab Chip* 2009, **9**, 802-809.

[54] Feldman, H. C., Sigurdson, M., Meinhart, C. D., *Lab Chip* 2007, **7**, 1553-1559.

[55] Wu, J., Lian, M., Yang, K., *Appl. Phys. Lett.* 2007, **90**, 234103.

[56] Gagnon, Z. R., Chang, H. C., *Appl. Phys. Lett.* 2009, **94**, 024101.

[57] Sabounchi, P., Huber, D. W., Kanouff, M. P., Harris, A. E., Simmons, B. A., *12th International Conferences on Miniaturized Systems for Chemistry and Life Sciences*, pp. 50-52, October 12-16, San Diego, California, USA.

[58] Hawkins, B. J., Kirby, B. J., *Electrophoresis* 2010, **31**, 3622–3633.

[59] Erickson, D., Sinton, D., Li, D., *Lab Chip* 2003, **3**, 141-149.

[60] Melcher, J. R., Taylor, G. I., *Annu. Rev. Fluid. Mech.* 1969, **1**, 111-146.

[61] Kirby, B. J., *Micro- and Nanoscale Fluid Mechanics: Transport in Microfluidic Devices*, Cambridge University press 2010.

[62] Xuan, X., Sinton, D., Li, D., *Int. J. Heat Mass Trans.* 2004, **47**, 3145–3157.

[63] Lide, D. R., *CRC handbook of chemistry and physics*, 90 ed., CRC Press, 2009.

[64] Xuan, X., Xu, B., Sinton, D., Li, D., *Lab Chip* 2004, **4**, 230-236.

[65] Tang, G., Yang, C., *Electrophoresis* 2006, **27**, 628-639.

[66] Kates, B., Ren, C. L., *Electrophoresis* 2006, **27**, 1967–1976.

[67] Ross, D., Gaitan, M., Locascio, L. E., *Anal. Chem.* 2001, **73**, 4117-4123.

[68] Shi, J., Mao, X., Ahmed, D., Colletti, A., and Huang, T. J., *Lab. Chip*., 2008, 8, 221-223.

[69] Zhao, Y., Fujimoto, B. S., Jeffries, G. D. M., Schiro, P. G., and Chiu, D. T., *Optics Express*, 2007, **15**, 6167-6176.

[70] Ramadan, Q., Samper, V., Poenar, D., and Yu, C., *Biomed. Microdev*., 2007, **8**, 151-158.

[71] Yu, C., Vykoukal, J., Vykoukal, D. M., Schwartz, J. A., Shi, L., and Gascoyne, P. R. C., *J. Microelectromech. Syst*., 2005, **15**, 480-487.

[72] Jen. C.P., Huang. C.T., and Weng. C.H., *Microelectronics Engineering*, 2010, **87**, 773-777

[73] Jeon. W., Shin. W. J., *Chemical Engineering Journal,* 2009, **152,** 575–582.

[74] Nguyen, N. T., Wu, Z, *J. Micromech. Microeng.* 2005, **15**, R1-R16.

[75] Schwesinger, N., Frank, T., Wurmus, H., *J. Micromech. Microeng.* 1996, **6**, 99–102

[76] Bessoth, F. G., deMello, A. J., Manz, A., *Anal. Commun.* 1999, **36**, 213-215.

[77] Stroock, A. D., Dertinger, S. K. W., Ajdari, A., et al., *Science* 2002, **295**, 647-651.

[78] Liu, R. H., Stremler, M. A., Sharp, K. V., et al., *J. Microelectromech. Syst.* 2000, **9**, 190–197.

[79] Kim, D., Lee, S., Kwon, T., Ahn, C. H., *Lab Chip,* 2005*,* **5**, 739–747.

[80] Sudarsan, A. P., Ugaz, V. M. , *Proc. Natl. Acad. Sci.* 2006, **103**, 7228-7233.

[81] Ahmed, D., Mao, X. Shi, J., et al, *Lab Chip* **9**, 2009, 2738-2741.

[82] Bau, H. H., Zhong, J., Yi, M., *Sens. Actuat. B,* 2001, **79**, 205-213.

[83] Chang, C., Yang, R., *Microfluid. Nanofluid, 2*007, **7**, 501-525.

[84] Garstecki, P., Fuerstman, M. J., Fischbach, M. A., et al *Lab Chip,* 2006 **6**, 207-212.

[85] Paik, P., Pamula, V. K., Fair, R. B, *Lab Chip,* 2003*,* **3**,253–259.

[86] Wu. Z., Li. D., *Electrochimica Acta*, 2008, 53, 5827–5835.

[87] Jeon.W., Shin. C.B., *Chemical Engineering Journal* 2009, **152**, 575–582

[88] Naher.S., *Simulation Modelling Practice and Theory*, 2011 **19,** 1088–1095